LHCb RICH 1 Engineering Design Review Report
Members of the LHCb RICH group

University of Bristol, Bristol, UK

N.H. Brook, R.D. Head, F. Metlica, A. Muir, A. Phillips, F.F. Wilson

University of Cambridge, Cambridge, UK

A. Buckley, V. Gibson, K. Harrison, C.R. Jones, S.G. Katvars, C. Lazzeroni, J. Storey,
C.P. Ward, S.A. Wotton

University of Milano-Bicocca and INFN, Milano, Italy

M. Alemi, C. Arnabaldi, T. Bellunato, M. Calvi, C. Matteuzzi, M. Musy, P. Negri, D. Perego,
G. Pessina

University of Edinburgh, Edinburgh, UK

R. Chamonal, S. Eisenhardt, J. Lawrence, J .McCarron, F. Muheim, S. Playfer, A. Walker

University of Genoa and INFN, Genoa, Italy

S. Cuneo, F. Fontanelli, V. Gracco, G. Mini, P. Musico, A. Petrolini, M. Sannino

University of Glasgow, Glasgow, UK

A.G. Bates, A. MacGregor, V. O'Shea, C. Parkes, S. Paterson, D. Petrie, A. Pickford,
M. Rahman, F.J.P. Soler[1]

Imperial College, London, UK

L. Allebone, G.J. Barber, W. Cameron, D. Clark, P. Dornan, A. Duane, U. Egede, R.Hallam,
A. Howard, R. Plackett, D.R. Price, T. Savidge, G. Vidal-Sitjes, D. Websdale

University of Oxford, Oxford, UK

M. Adinolfi, J.H. Bibby, C. Cioffi, V. Gligorov, N. Harnew, F. Harris, I.A. McArthur,
C. Newby, B. Ottewell, J. Rademacker, R. Senanayake, L. Somerville, A. Soroko, N.J. Smale,
S. Topp-Jorgensen, G. Wilkinson, S.Yang

University of Paris VI and VII (LPNHE) Paris, France

M. Benayoun

Institute of High Energy Physics (IHEP-Serphukov), Protvino, Russia

V .Khmelnikov, V .Obraztsov

Rutherford Appleton Laboratory, Chilton, UK

C.J. Densham, S. Easo, B. Franek, G. Kuznetsov, P. Loveridge, D. Morrow, J.V. Morris,
A. Papanestis, G.N. Patrick, M.L. Woodward

CERN, Geneva, Switzerland

G. Aglieri-Rinella, A. Albrecht, A. Braem, M. Campbell, C. D'Ambrosio, R. Forty, C. Frei,
T. Gys, O. Jamet, N. Kanaya, M. Losasso, M. Moritz, M. Patel, D. Piedigrossi, W. Snoeys,
O. Ullaland, A. van Lysebetten, K. Wyllie,

[1] also at Rutherford Appleton Laboratory, Chilton

Abstract

This document describes the concepts of the engineering design to be adopted for the upstream
Ring Imaging Cherenkov detector (RICH 1) of the reoptimized LHCb detector. Our aim is to
ensure that coherent solutions for the engineering design and integration for all components of
RICH 1 are available, before proceeding with the detailed design of these components.
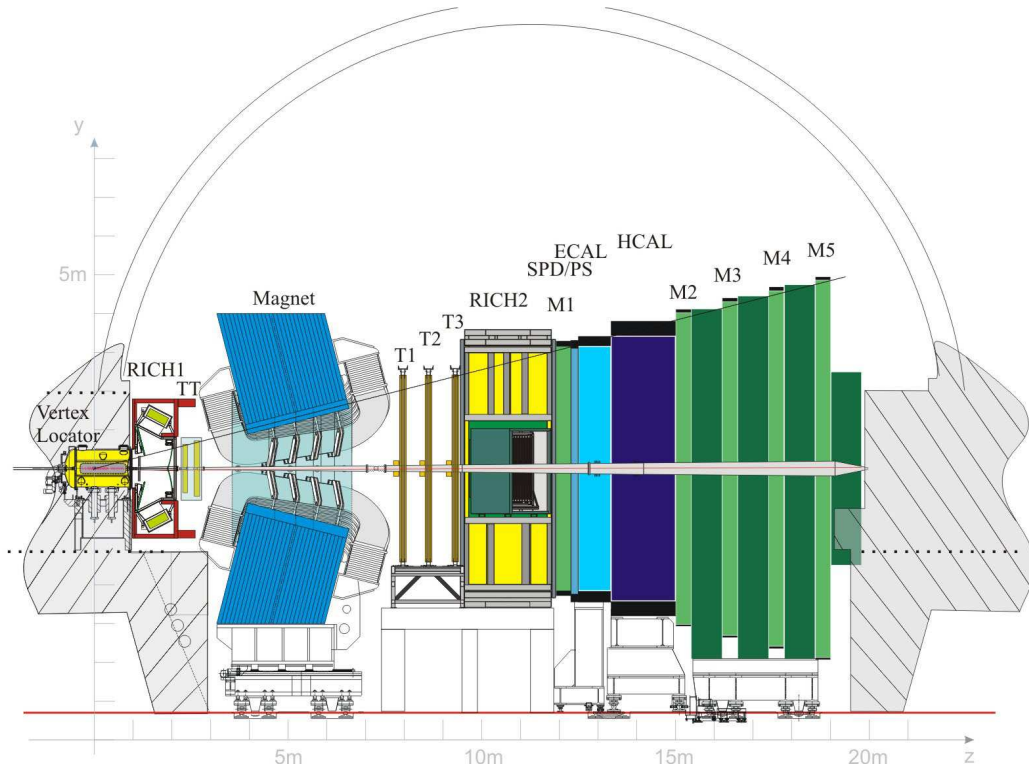
Contents

Figure 1: Reoptimized LHCb detector layout, showing the two RICH detectors. RICH 1 is located upstream of the LHCb dipole magnet, between the VELO and Trigger Tracker.

1 Introduction

The layout of the LHCb detector is shown in Fig. 1 and described in the Reoptimized Detector Design and Performance Technical Design Report (TDR) [1]. Particle identification is provided by two Ring Imaging Cherenkov (RICH) detectors. The basic requirement for the RICH system is to provide particle identification over a wide momentum range, from $1- \geq 100 \, \text{GeV}/c$. The technical design of the system has been described in TDRs [1, 2] and the engineering design of RICH 2 is described in reference [5]. This report describes the engineering design solutions chosen for the RICH 1 detector. It does not include detailed production engineering drawings; these will be included in the production readiness reviews that precede ordering and manufacture of the component subsystems. The photon detectors are described in an addendum to the RICH TDR [3] and their readout electronics have been the subject of an independent review report [4].

RICH 1 is shown in Fig.1 upstream of the LHCb dipole magnet, between the VELO and Trigger Tracker (TT). It contains silica aerogel and fluorobutane (C_4F_{10}) gas radiators, providing particle identification from $1 - 60 \, \text{GeV}/c$ for particles within a polar angle acceptance of $300 \, \text{mrad}$ (horizontal) and $250 \, \text{mrad}$ (vertical).

The LHCb coordinate system is right-handed, with origin at the interaction point (IP). The z-axis follows the beam line which is inclined at $+3.6 \, \text{mrad}$ to the horizontal, the y-axis points upwards, orthogonal to the z-axis, and the x-axis is horizontal. RICH 1 is aligned to the LHCb coordinate axes and is placed within the limits $985 \leq z \leq 2170 \, \text{mm}$, assigned by the LHCb Detector Geometry Database [6]. The gas Cherenkov radiator, C_4F_{10}, has refractive index $n = 1.015$ at STP and is operated at atmospheric temperature and pressure. The silica aerogel has refractive index $n = 1.03$ and provides positive kaon identification from $2 - 10 \, \text{GeV}/c$. The Cherenkov angle as a function of particle momentum is shown for the RICH system radiators in Fig. 2. In addition to the particle identification (PID) requirements, other criteria have mo-
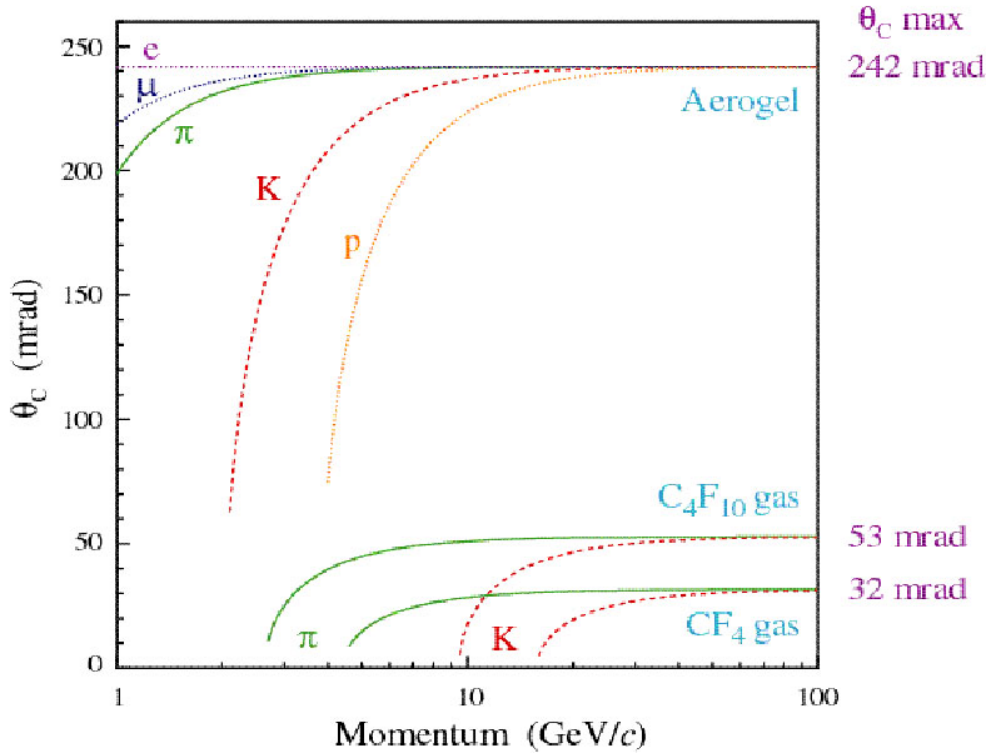
Figure 2: Cherenkov angle as a function of particle momentum for the radiators of the LHCb RICH system.

tivated the solutions adopted for the RICH 1 engineering design. These include:

Material budget

Minimizing the material within the particle acceptance of RICH 1 has driven us to use beryllium for the substrate of the spherical mirrors. All other components of the optical system are located outside of the acceptance. The exit windows are constructed from a carbon-fibre skinned foam sandwich panel and the entrance window is eliminated by sealing the gas enclosure directly to the VELO tank. The contributions to the RICH 1 material budget that fall within the acceptance are listed in Table 1.

Table 1: Contributions (expressed as fractions of a radiation length and nuclear interaction length) to the material in RICH 1, that fall within the LHCb acceptance.

Item	X_0	λ_I
Aerogel	0.033	0.007
Gas radiator	0.026	0.016
Spherical mirror (Be)	0.008	0.007
Exit window	0.006	0.003
Total (with Be mirror)	0.073	0.033

Interface to the LHC beampipe

The low angle acceptance of RICH 1 is limited by the 25 mrad section of the LHC beampipe which passes through the detector. The installation of the beampipe and the provision of access required for its bake-out have motivated several features of the RICH 1 design.

4

Magnetic shield for photon detectors

The Hybrid photon detectors (HPDs) of the RICH detectors need to be shielded from the fringe field of the LHCb dipole. In the absence of shielding this field is about 60 mT and iron shielding boxes are required to attenuate the field to a level of 2.5 mT where HPDs can operate within individual Mumetal shields. The iron shields are also used to extract flux from the dipole and focus it into the tracking region where magnetic bending power is required for the Level-1 trigger [7].

1.1 Evolution since the RICH Technical Design Report

The overall reoptimization of the LHCb detector has had major consequences on the design of RICH 1, with respect to that described in the RICH TDR. Most of these changes were addressed in Chapter 4 of the reoptimized TDR [1] but at the time that document was written the multi-anode PMT was the baseline photon detector choice. In the interest of clarity and completeness we list below the main changes in the RICH 1 design with respect to the RICH TDR.

- Additional plane mirrors (as in RICH 2) are required so that the HPDs can be located in a region where iron magnetic shielding can be used.

- Horizontally-located iron shields would steal the B-field away from where it is required by the Level-1 trigger, so the HPDs are located above and below the beam where the shields can focus the field. Hence the new RICH 1 design employs a vertical optical layout as shown schematically in Fig. 3(a).

- Reduction of the material budget is achieved through the use of beryllium spherical mirrors with supports and adjustment mechanism outside the spectrometer acceptance. The entrance window is eliminated by sealing the gas volume directly to the VELO. In Fig. 3(b) a cut-away 3D model of the RICH 1 detector is shown, attached by a gas-tight seal to the VELO tank. The labelling on this figure refers to the components that are described in the following sections of this report.

2 Parameters of the Optical System

The parameters of the RICH 1 optical layout have been studied with the aid of both GEANT4 and stand-alone simulations. The upper and lower halves are symmetric about the plane $y = 0$, however Cherenkov photons emitted by upward-going charged tracks can be detected in the lower HPDs, so the full acceptance is simulated. There is also reflection symmetry about the plane $x = 0$, and the mirrors and HPD plane are tilted only in the $y - z$ projection: the centres of curvature of the spherical mirrors and the normals through the centres of the flat mirrors and the HPD planes therefore all lie in the plane $x = 0$.

2.1 Method

High momentum charged tracks are simulated, originating from the IP and passing through the active LHCb acceptance (with polar angles $|\theta_x| \leq 300$ mrad, $0 \leq \theta_y \leq 250$ mrad in the $x - z$ and $y - z$ projections respectively). A uniform distribution of tracks is generated within these limits.
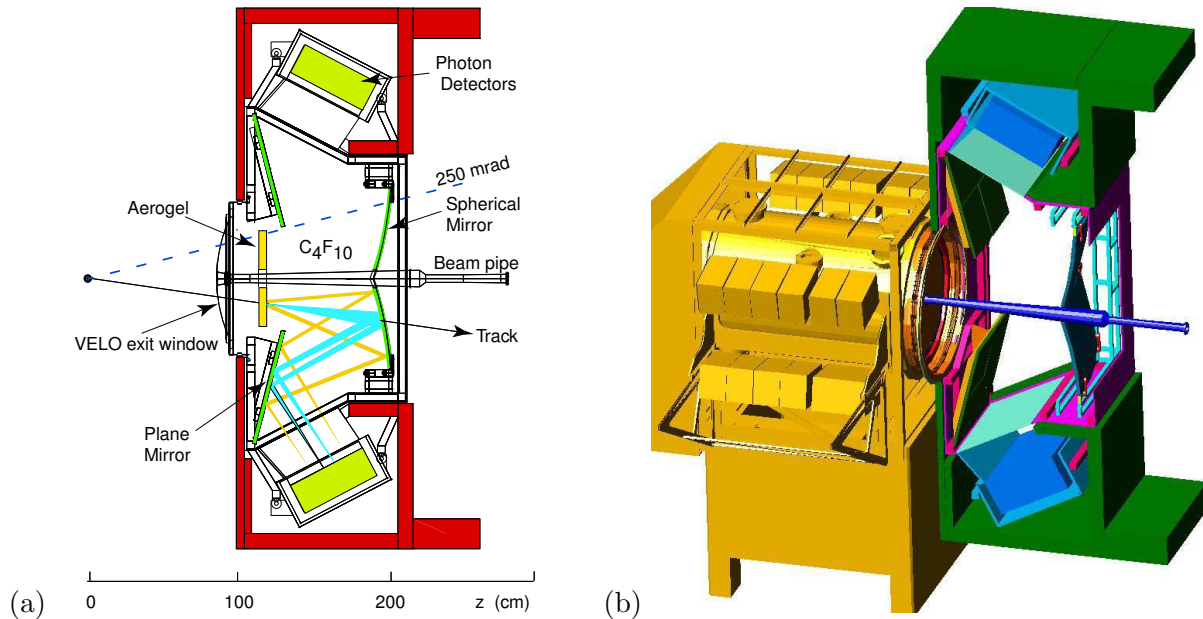
Figure 3: (a) Schematic layout of the RICH 1 detector [Some details in this figure are not up-to-date].
(b) Cut-away 3D model of the RICH 1 detector, shown attached by its gas-tight seal to the VELO tank.

Cherenkov photons are generated uniformly along the length of each track within the aerogel and gas radiators, using the appropriate refractive index for photons within the wavelength acceptance of the HPD photocathodes. The average polar Cherenkov angle is 240 mrad for aerogel and 53 mrad for the C_4F_{10} gas radiator. The azimuthal angle is uniformly distributed. All photons are ray traced, reflecting off the spherical and flat mirrors, and their impact on the HPD plane is recorded. Photons that strike the LHC beampipe and other obstructions are considered to be lost. A typical track and its generated photons is displayed in Fig. 4.

The Cherenkov angle at emission is then reconstructed for each photon in turn, using the procedure developed for off-line analysis: the HPD impact point is used together with knowledge of the optics to calculate the Cherenkov angle. For this it is assumed that the emission point is midway along the corresponding track in the radiator. As the true emission point is randomly distributed along the track the reconstructed angle will not agree exactly with the true value. If the optical system were configured as an ideal RICH system, then all photons emitted at a given azimuthal angle would be focused to the same point on the HPD plane. Tilted mirrors result in non-ideal optics and the smearing of the reconstructed Cherenkov angle distribution provides a measure of the quality of the focusing. Its RMS is referred to as the emission-point error. The RICH 1 optics is designed such that the emission-point error is not larger than other sources of finite angular resolution, such as the HPD pixel size and the chromatic dispersion due to the variation in refractive index of the radiator with wavelength. The pixel size of the HPD (2.5 mm at the photocathode) results in a contribution of 0.6 mrad to the Cherenkov angle precision, while chromatic dispersion contributes 0.8(1.6) mrad in the gas(aerogel) radiators. These values set the targets for the emission-point error of the optical system.

In addition to the emission-point error, the optical layout determines the required area of coverage by the HPD plane. In the interest of cost this area should be reduced. In the optimization procedure we have required a 100% acceptance for photons emitted by the gas radiator, while a compromise (cost/PID performance) has been accepted for the aerogel photons.

Several constraints from the mechanical construction and magnetic shielding need to be respected
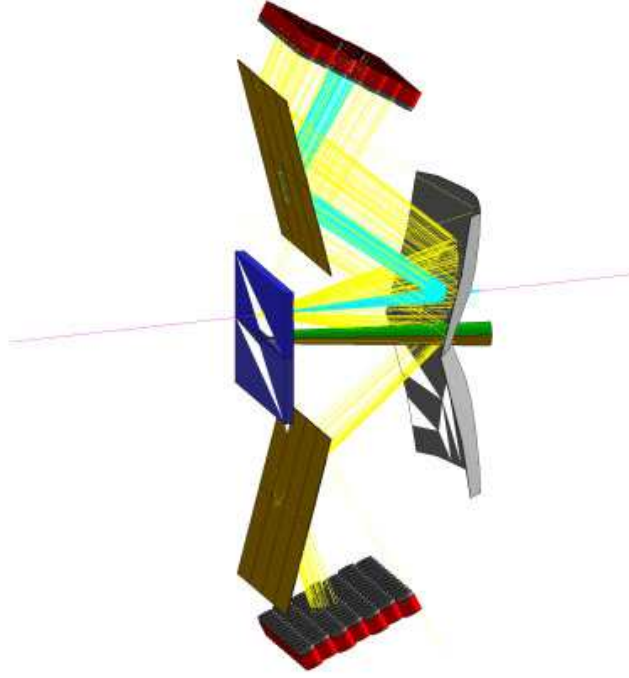
6

Figure 4: GEANT4 display of Cherenkov photons emitted from aerogel and gas radiators by a charged track. The photons are reflected from spherical and plane mirrors, traverse the quartz windows and strike the HPDs.

as discussed below. The parameters that have been adjusted include: the spherical mirror radius, location of its centre of curvature, location and tilt of the plane mirror and of the HPD plane, as well as the boundaries of these components.

2.2 Constraints

The z-coordinates of the optical elements are constrained by the requirement that RICH 1 fits within the envelope assigned to it within the LHCb detector. Space must be allowed for the finite dimensions of the mirrors and their support structures as well as the thicknesses of the magnetic shielding, the gas enclosure and the exit window. After accounting for these contributions the reflective suface of the spherical mirror must lie at $z \leq 2085$ mm and the reflective surface of the flat mirror must lie at $z \geq 1090$ mm.

The tilt of the spherical mirror must ensure that the flat mirror lies outside the particle-acceptance of RICH 1, i.e. $y > z \tan 0.25$. The location of the HPD plane is determined by the performance of the magnetic shield box. The HPDs must be located within the shield such that the maximum field experienced is 2.5 mT. The tilt of the HPD plane is chosen to ensure that, on average, Cherenkov photons strike the HPDs at close to normal incidence.

2.3 Results

The parameters chosen are listed here, rounded to the nearest mm and mrad. The corresponding coordinates of the optical components are listed and displayed in Fig. 5.

- The spherical mirrors have radius of curvature 2700 mm with centres of curvature at
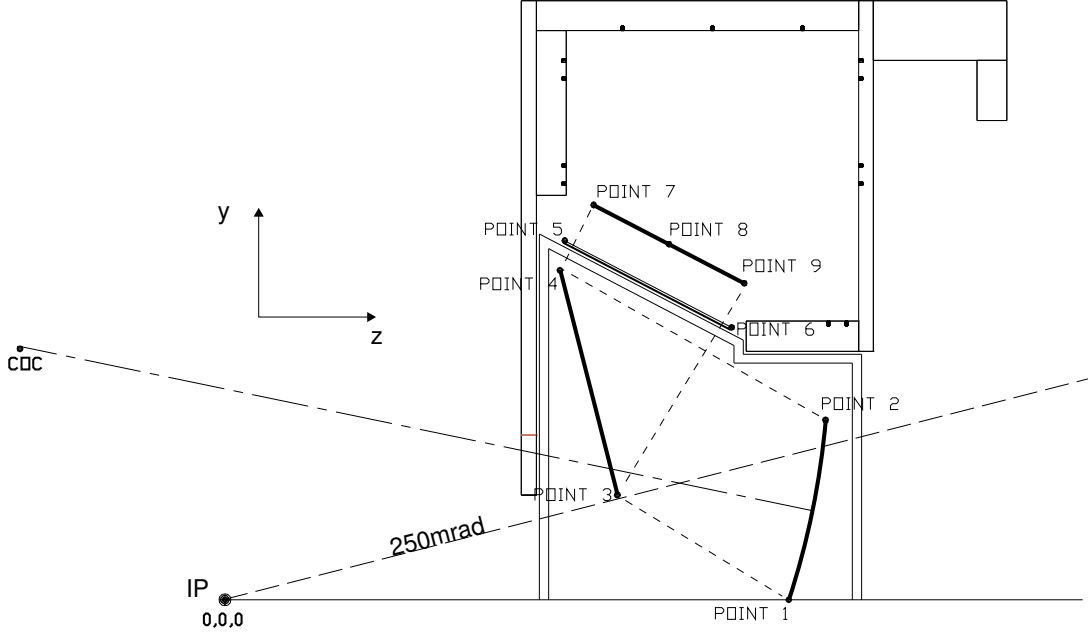
Figure 5: Half view of the optical geometry in the plane $x = 0$. Coordinates (y, z in mm) for the indicated points are:
Centre of curvature (837.9, -684.4),
Spherical mirror: point 1 (0.0, 1882.3), point 2 (600.0, 2005.1),
Plane mirror: point 3 (350.0, 1310.0), point 4 (1100.0, 1118.5),
Quartz window: point 5 (1191.1, 1134.51), point 6 (909.5, 1691.7),
HPD plane: point 7 (1317.7, 1231.7), point 8 (1187.4, 1482.3), point 9 (1056.7, 1733.8).

   $x, y, z = 0, \pm 838, -684$ mm.
   Their boundaries in the $x - y$ projection are given by $x = \pm 795$ mm, $y = 0, \ 600$ mm and similarly for the lower ($-y$) mirror.

- The flat mirrors are tilted at an angle 0.250 rad with respect to the y-axis.
  Their boundaries in the $x - y$ projection are given by $x = \pm 740$ mm, $y = 350, \ 1100$ mm and similarly for the lower ($-y$) mirror.
  Their horizontal edges that lie closest to the beam line are located at $z = 1310$ mm.

- The HPD planes are centred at $x, y, z = 0, 1187, 1482$ mm and tilted at an angle 1.091 rad with respect to the y-axis. They are covered by 7 rows of 14 HPDs, hexagonally close packed, with centres separated by 91.5mm. This corresponds to an area for the HPD plane of $1327 \, \text{mm} \times 567 \, \text{mm}$, with an active area fraction of 0.61.

With these parameters, the emission-point error is an acceptable value of 0.67 mrad for the gas radiator, and negligible compared with other sources of error for the aerogel. The photon hit density distributions at the mirrors and HPD plane are shown in Fig. 6. These show that the mirror dimensions given above are more than adequate to ensure that all photons that potentially fall within the HPD acceptance can be reflected. The fraction of photons generated by the gas(aerogel) and striking the HPD plane is 100%(68%) and striking an active photocathode is 61%(42%). The numbers of photoelectrons detected per track has been estimated [1] at $N_{pe} = 30(6)$ for the gas(aerogel) radiators respectively.
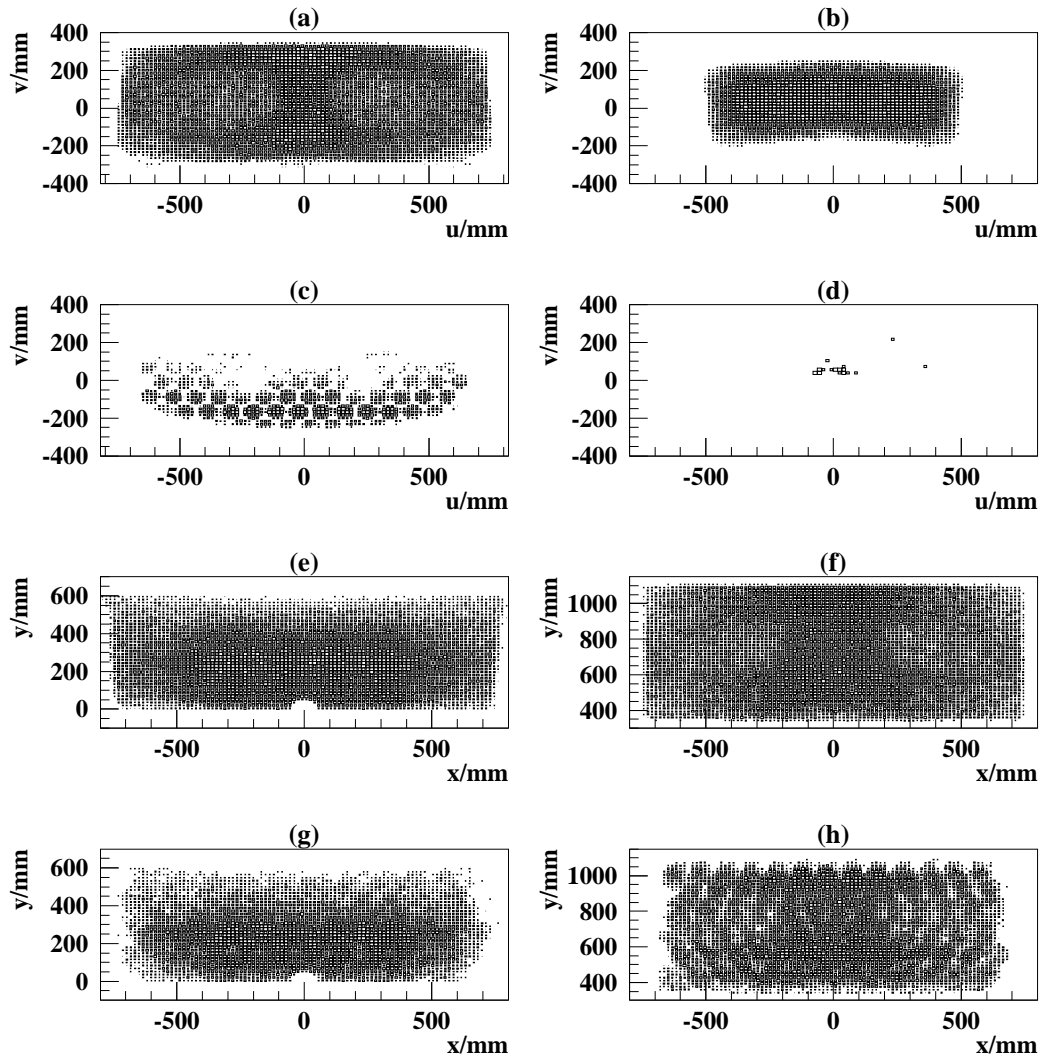
8

Figure 6: Hit density distributions of the impact point of simulated photons on various surfaces, where the area of each box is proportional to the number of photons landing in that region and the axes refer to coordinates in the LHCb reference system. Only upward-going tracks are used to generate the Cherenkov photons:
(a) Aerogel and (b) C_4F_{10} photon hits on upper HPD plane.
(c) Aerogel and (d) C_4F_{10} photon hits on lower HPD photocathodes.
(e) Spherical and (f) plane mirror hits for all photons in LHCb acceptance.
(g) Spherical and (h) plane mirror hits for photons that hit HPD photocathodes.

Within the constraints of the current design it is possible to move this optical system by $50\,mm$ in z, keeping all other parameters fixed. The final z-location could retain this flexibility until the testing of prototype mirror adjustment mechanisms is completed and their detailed design is frozen (Feb 2005).
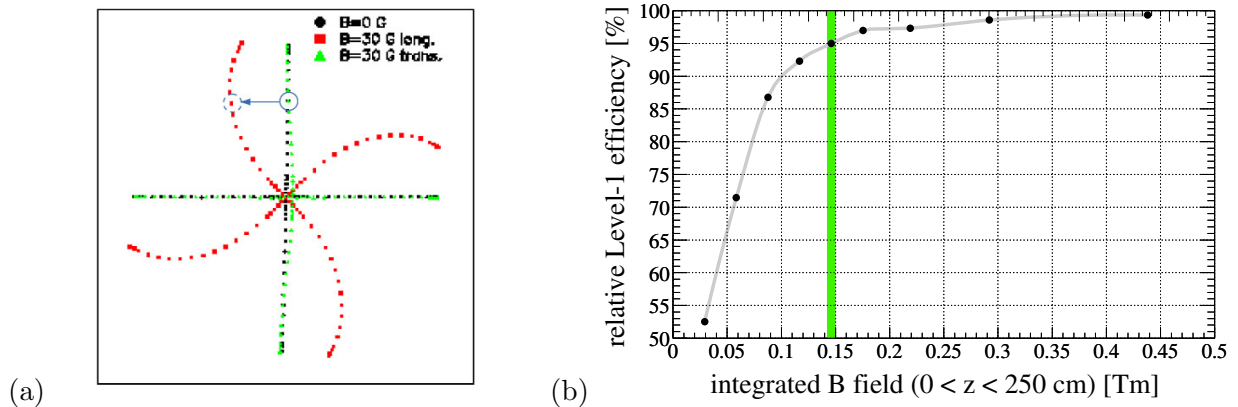
Figure 7: (a)Effect of a 3 mT magnetic field on the HPD image; the image of a cross on the anode is shown for no applied field, and then for 3 mT axial and transverse fields. The square boundary represents the 16 mm×16 mm sensitive area of the pixel sensor, and the largest observed translation (about 2.5 mm = 5 pixels) is indicated with an arrow.
(b)Dependence of the Level-1 trigger performance on the upstream magnetic bending. The vertical line corresponds to the field integral used in recent physics performance studies.

3 Magnetic Shield

In the absence of magnetic shielding the HPDs would experience a magnetic field from the LHCb dipole of about 60 mT. HPDs have been tested in both axial and transverse magnetic fields. The distortions of the electron optics, primarily a rotation of the image due to the axial component, is shown in Fig. 7(a) for a single HPD, surrounded by a 0.9 mm-thick coaxial Mumetal cylinder, in B-fields of 3 mT, both axial and transverse. Although the distortions need to be corrected (this is described in an addendum to the RICH TDR [3]), there is no loss of the image from the active area of the pixellated anode. With an axial field of 5 mT there is a loss of about 4% of the photocathode area. A 5 mT transverse field results in no loss. Measurements have been made of the field inside an array of Mumetal shields with an external axial field of 5 mT. These indicate that the field inside the HPD is equivalent to that seen by a single shielded tube at 3 mT. Transverse fields give small distortions but the array is more difficult to shield due to possible saturation of the Mumetal tube array. A preliminary analysis using an array of 0.9 mm-thick Mumetal cylinders in the RICH 1 shield indicates that the field inside the cylinders does not exceed 1 mT, while the field in the Mumetal itself is 0.35 T, about one half the saturation value. Until we have experimental confirmation, this risk is mitigated in the current RICH 1 design by allowing space in the HPD assembly for Mumetal shields up to 2 mm thick.

The bending of charged particles in the fringe field between the VELO (where the magnetic field must be small) and the TT station is an important requirement in the Level-1 trigger. The degradation of the Level-1 trigger performance as a function of this bending is shown in Fig. 7(b), with further details in [7].

3.1 Requirements

The design goal for the iron magnetic shielding boxes has been to reduce the magnetic field everywhere in the plane of the HPDs (B_{max}) to < 2.5 mT, while maintaining a field integral along the z-axis from 0 to 2500 mm (B_{trig}) of > 0.15 T·m.

The engineering design is constrained by several other factors including the obvious need for space to accommodate the HPDs and their readout electronics and for an unobstructed light path

10

to the HPDs. The available space envelope must be respected and gravitational and magnetic forces must be accommodated in the design. Since the HPD assemblies and the gas enclosure are mounted from the shielding boxes they will need to be mechanically stable at the level of 0.5 mm (cf: HPD pixel size of 2.5 mm), to avoid degrading the Cherenkov angular precision. The assembly of the beampipe to the VELO and the subsequent sealing of the RICH 1 gas enclosure at the VELO exit window requires that the upstream walls cannot approach closer than 550 mm to the beampipe at $x = 0$, although some shaping around the aperture (teeth) of the circular window is possible.

Availability of the raw ARMCO iron (the preferred shielding material) in thicknesses of 50 and 100 mm has been taken into account to reduce machining costs. Furthermore, the limited craning facilities at the location of RICH 1 have motivated a design of the lowest possible weight. Removable parts are required for access to the HPDs, to the mirror assemblies and to the beampipe. Bake-out of the beampipe requires removal of the mirror assemblies. Again, limited crane facilities dictate that the weight of each removable part should not exceed about one tonne.

3.2 Magnetic Modelling

The shielding has been designed with the aid of the TOSCA/OPERA[1] finite element software package in which the complete LHCb dipole is modelled as well as the shield. This has allowed a good understanding of the effect of varying the design parameters (details can be found in [1]), although absolute values of the fields predicted by the model have not been checked experimentally, and will not be until the shields have been manufactured and installed in the B-field of the LHCb dipole. The meshing of the model has been varied and indications are that absolute predictions are stable at the level of 10–20%. One global conclusion from the model is that any change required to increase the field integral also increases the field inside the shielding. The resolution of these conflicting goals is only achieved by adding iron extension blocks between the shielding boxes and the LHCb magnet. These collect flux from the magnet, channel it through the shield box and the upstream pole directs it where it is needed for the trigger.

The model, resulting from an iterative optimization procedure, is shown in Fig. 8. The shielding boxes are constructed from very pure (ARMCO) iron with a high saturation field $\sim$1.8 T. Their essential components are illustrated in the figure and comments listed below:

- *Top plate:* 100 mm thick; if thinner, results in saturation.

- *Pole piece:* 50 mm-thick upstream plate. Its vertical dimensions are critical to both HPD shielding and bending power. The closer to the beam line the better the magnetic performance.

- *Side plates:* 50 mm thick. Need to be removed for access, therefore thin to reduce weight. 400 mm×400 mm cut-out for HPD services.

- *Teeth:* 50 mm thick; improve magnetic performance

- *Downstream plate:* 50 mm thick; channels fringe field from magnet away from HPDs. No advantage if thicker.

- *Internal block:* 100 mm thick; improves performance of pole piece, enhancing B_{trig}.

- *Shelf:* 100 mm thick; reduces aperture of window in front of HPDs, reducing B_{max}.

- *Extension blocks:* 200 mm thick; critical to the trigger field, act as a funnel for magnetic flux and channel flux to pole the piece.
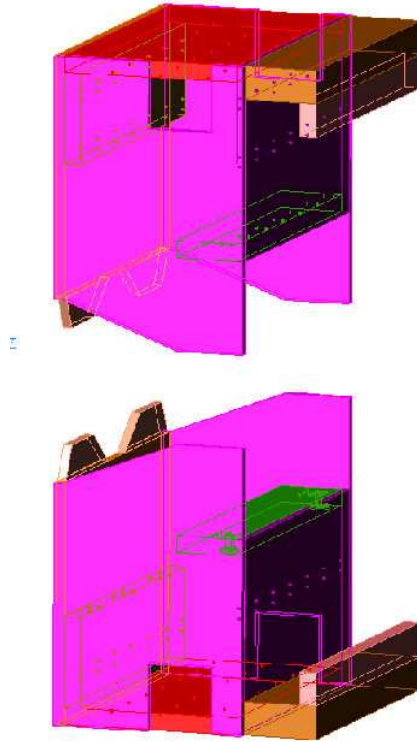
Figure 8: RICH 1 magnetic shielding boxes.

Results of the magnetic analysis for these shielding boxes are shown in Fig. 9. The maximum field at the photon detector plane is B_{max}=2.6 mT and is directed such that the main component is axial for most HPDs. The integral field B_{trig}=0.14 T·m. These values are close to the design goals and represent the best compromise we can achieve for the conflicting requirements. The magnetic forces on this structure have been calculated by integrating the Maxwell stress tensor over the surface. The horizontal force on each box (towards the magnet) is 35 kN and the vertical component (directed up(down)wards on the upper(lower) box) is 26 kN. These are comparable to the weight (approx 8 tonnes per box) and are accounted for in the mechanical design.

3.3 Mechanical Construction

The mechanical design is required to conform to the components of the shield as described by the magnetic model. It must also provide the interfaces to other parts of the RICH 1 detector and provide facilities for its assembly. These include:

- Support to attach upper to lower shielding boxes during installation

- Mounting of lower box to tunnel floor

- Mounting of upper box from cavern wall

- Craning points for removable parts

- Mounting points for HPD assembly support

- Mounting points for gas enclosure

An assembly diagram of the shielding structure is illustrated in Fig. 10. It shows the upper

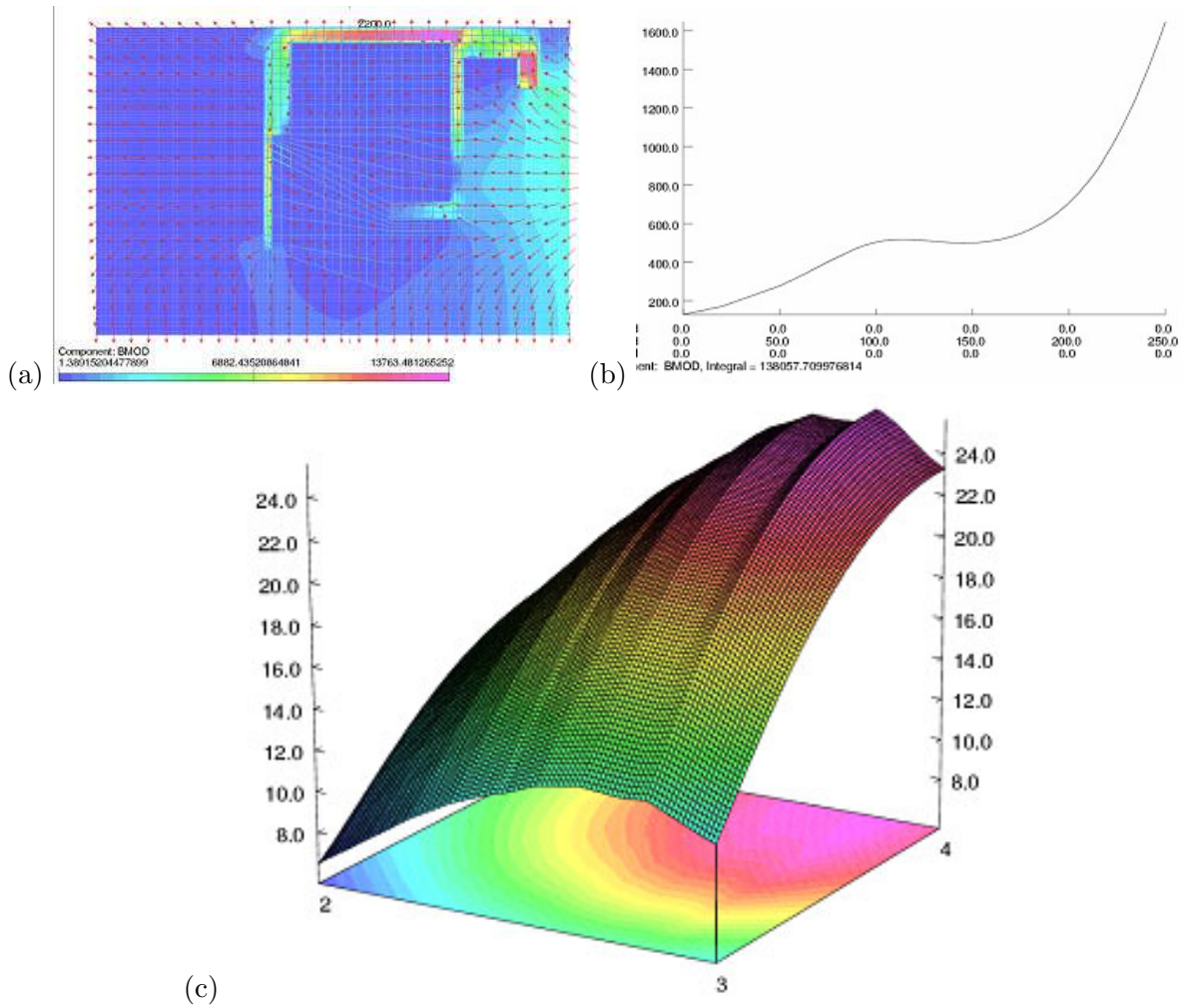---

[1]Vector Fields plc, Oxford, UK

(a)

(b)

(c)

Figure 9: Results from the TOSCA magnetic analysis.
(a) B-field through the vertical cross section of the shield at $x = 0$. The magnet coils are close to the top right-hand corner of the box, from where flux is channelled via the extension block through the top of the shielding box and down the upstream pole. The arrows indicate the direction of the field, its magnitude is indicated by the colour-coding.
(b) B-field along the beam line.
(c) Inside the box the HPDs experience a field whose main component is axial. The plot shows the magnitude (in gauss) of the B-field at the HPD plane.

box supported from the lower using four vertical beams. In this configuration the shield will be transported to its location in LHCb. The lower box is fixed to an adjustable mount on the tunnel floor (400 mm of concrete has already been cut away from the floor to accommodate the RICH1 shielding design as described), where it is positioned with a precision of order 1 mm. The upper box is then fixed to the cavern wall. The support beams are then removed.

Both boxes are assembled from 50 mm and 100 mm-thick plates of ARMCO iron. The main dimensions can be extracted from the coordinates tabulated in Table 2 together with Fig. 11. The weight of each box is approximately eight tonnes. The side walls are removable to allow access to the the HPD assemblies and to the gas enclosure. Craning points are provided to lower(raise) the side walls of the upper(lower) box, while the services (cooling and cables) of the HPDs remain connected. The HPD assemblies are mounted within the boxes from rails that allow travel in the x-direction for maintenance. Figure 12(a) shows the upper module to illustrate the concept. The upstream rail provides the reference positioning, while the downstream rail provides a constraint only in the y-direction. The support points are shown in Fig. 12(b). The

13
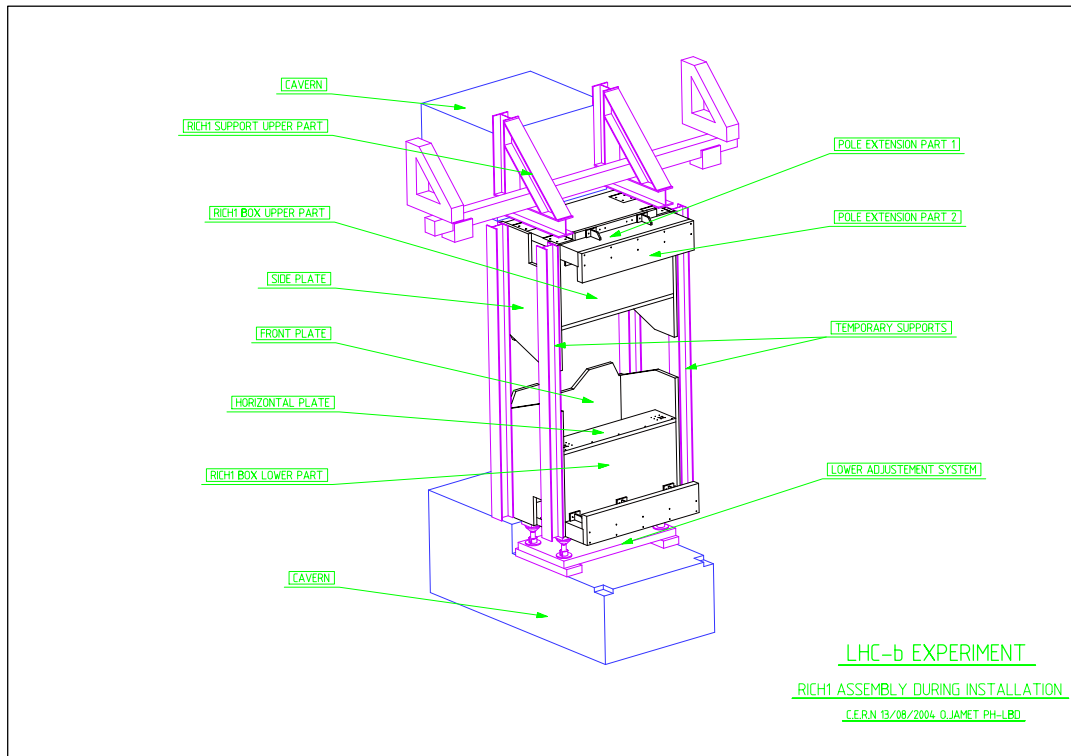
Figure 10: Assembly drawing of upper and lower shielding boxes held together by four temporary vertical beams during transport and installation. The lower box is fixed to adjustable mountings on the tunnel floor, while the upper box is hung from the cavern wall.
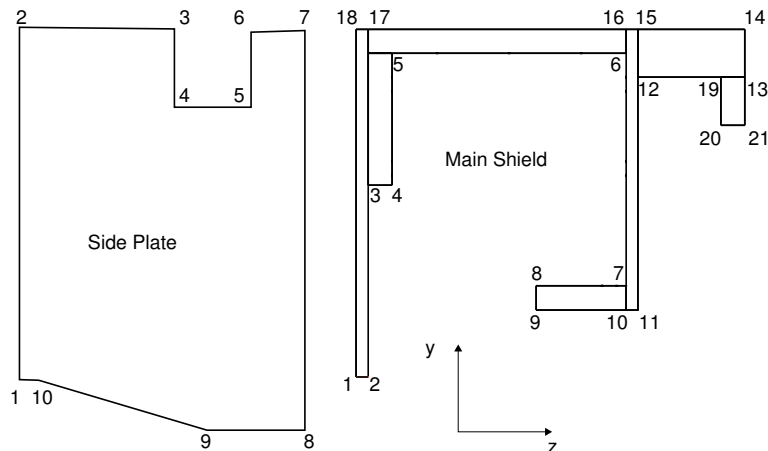
Figure 11: Outline of RICH 1 shield components. The coordinates of the points are give in Table 2.

gas enclosure is supported from the lower shielding box; it is not in mechanical contact with the upper box. A 10 mm clearance betwen the enclosure and the shield provides installation tolerance. Mounting points are provided on the shelf and on the front plate(pole piece). The mounting of the spherical mirrors within the gas enclosure restricts the space available for the downstream mountings of the gas enclosure and they need to be located either within the gas enclosure envelope or within the shelf of the shielding box. The design illustrated in Fig. 13 accommodates either solution. A temporary guide rail is attached to the shields to facilitate the installation of the gas enclosure onto these mountings.

Table 2: Coordinates (in mm) in the LHCb system for components of the upper shielding box. The lower box has the sign of the y-coordinate reversed.

| Main Shielding components				Side Plate			
Point	x	y	z	Point	x	y	z
1	± 925	550	990	1	Inside ± 925 Outside ± 975	550	990
2		550	1040	2		2000	990
3		1350	1040	3		2000	1577.5
4		1350	1140	4		1600	1577.5
5		1900	1140	5		1600	1977.5
6		1900	2115	6		2000	1977.5
7		930	2115	7		2000	2165
8		930	1740	8		280	2165
9		830	1740	9		280	1760
10		830	2115	10		550	1040
11		830	2165				
12		1800	2165				
13		1800	2610				
14		2000	2610				
15		2000	2165				
16		2000	2115				
17		2000	1040				
18		2000	990				
19		1800	2510				
20		1600	2510				
21		1600	2610				
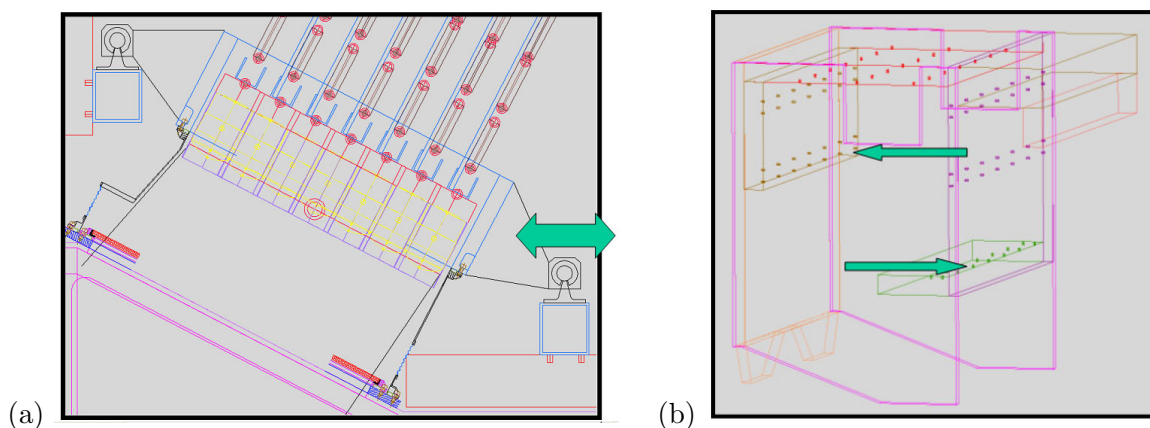
Figure 12: (a) Concept of HPD mounting in upper box. Rails fixed to the upstream (left) of the shield provide precise positioning of the HPD assembly. The right hand rail supports the weight and allows freedom as indicated by the arrow.
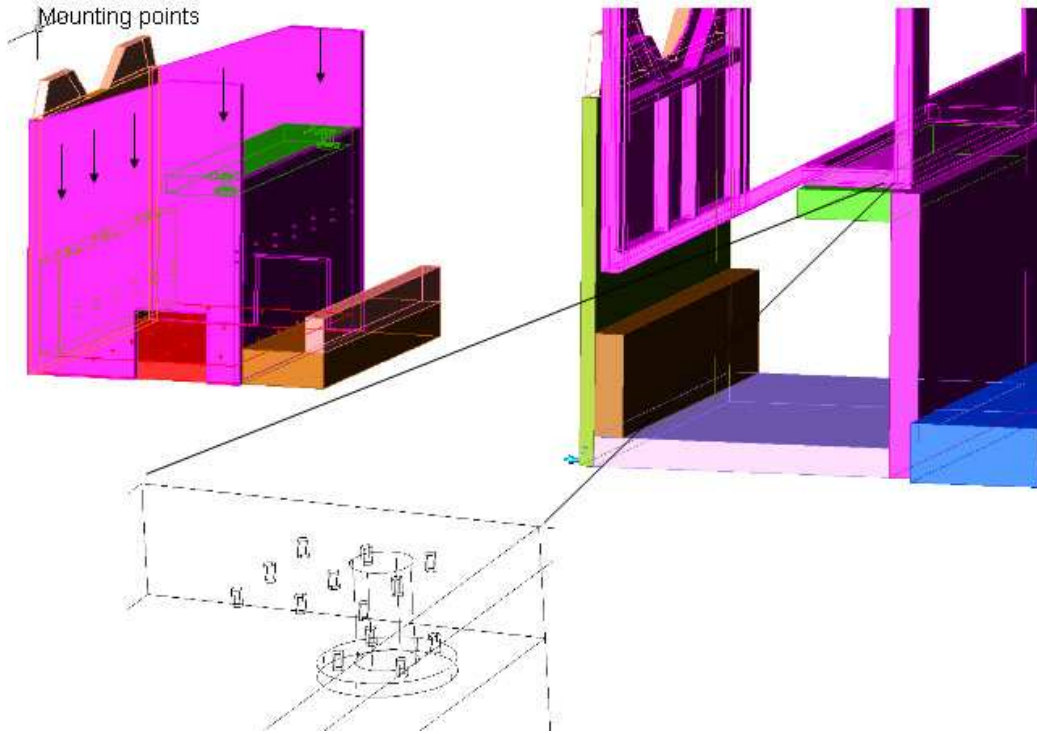(b) Mounting points in shielding box for HPD rails.

Figure 13: Mounting points in the lower shielding box for the gas enclosure.

4 Gas enclosure

4.1 Requirements

The major functions of the gas enclosure are to provide containment for the RICH 1 fluorocarbon gas radiator and to act as the stable platform for the optical components (the mirrors and aerogel). It must also be light tight. To ensure the stability of the structure under the influence of the magnetic field, all component parts are non-magnetic. The inside surfaces are blackened to reduce background from scattered photons. The operating pressure of the gas will be close to atmospheric (this is ensured by the gas recirculation system) but the enclosure must withstand a possible ± 3 mbar differential without compromising the mirror alignment. The minimum amount of material must be placed within the LHCb experiment acceptance limits.

The gas enclosure is supported by (and clamped to) the lower iron shield using adjustable mounts which accommodate the requirement to align the gas enclosure to the nominal beam position. These mounts are the only external points of contact and a nominal clearance to the iron shielding boxes of 10 mm all round has been imposed. The installation sequence requires that the gas enclosure be installed after the iron shields are already in place and aligned, so lifting points and an installation rail are foreseen. The beampipe is mounted by inserting it through the upstream and downstream faces so the enclosure must be in place before the beampipe installation can proceed. A recent change of installation strategy is the removal of the requirement to displace RICH 1 downstream for installation of the beampipe. Clearly the gas enclosure remains in place during beampipe bake-out. The weight load on the gas enclosure is due only to the mirror assemblies and the aerogel mounting, in total about 50 kg (the weight of the upper photon detector assembly, about 500 kg, is supported from the upper iron shield).
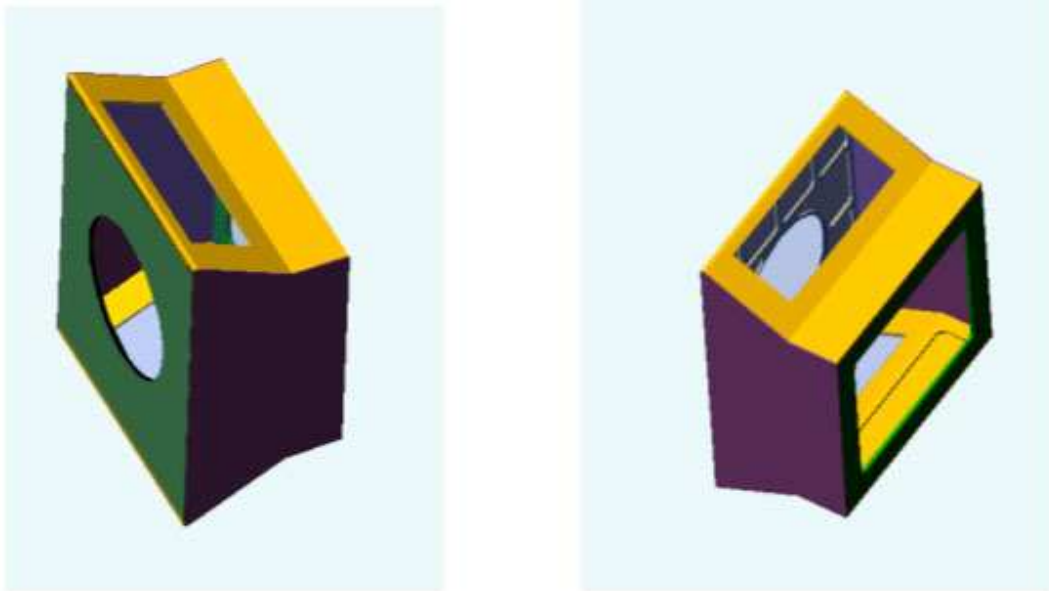
Figure 14: The gas enclosure, a monocoque construction manufactured from welded panels of 30 mm-thick aluminium tooling plate.

4.2 Mechanics

The gas enclosure is essentially a six-sided box (Fig.14) with each face closed by components having very different requirements:

- The upstream face is closed by an element which maintains the gas and light seal between the enclosure and the VELO exit face. This structure must also ensure that minimal force is exerted on the VELO and the upstream wall of the enclosure and that manufacturing and alignment tolerances (and changes due to temperature) can be accommodated.

- The top and bottom faces are closed by quartz windows that allow Cherenkov photons to pass through to the photon detectors mounted behind.

- The downstream face accommodates the low-mass exit window which is sealed to a flange on the beryllium beampipe.

- The side faces are closed by panels that are designed to maximize the access for installation of the internal optical components and the beampipe.

Recently it has been shown that the original frame-and-skin design of this box can be replaced with a design where each face of the structure is machined from 30 mm-thick aluminium-alloy tooling plate[2] which is then welded at the edges to form the enclosure. Although material costs of such an approach are higher, all necessary mounting, sealing and welding features can be machined into the plate at essentially a fixed cost. The weight of the gas enclosure is approximately 500 kg.

The dimensions of the entrance and exit windows are dictated primarily by the LHCb acceptance limits but the installation sequence imposes its own constraints. The VELO exit window, which is integral with the beampipe, must be able to pass through the gas enclosure entrance window, as must its clamping flange which is a complete ring. Both of these are able to pass through the gas enclosure seal to the VELO to allow for the possibility that this latter component is
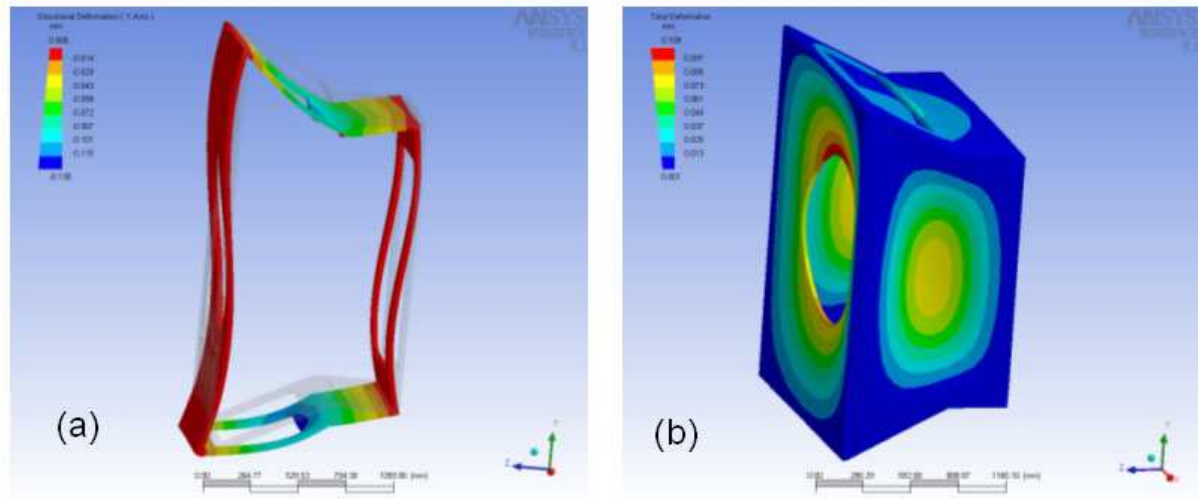
---

[2]6061-T651

Figure 15: FEA for the gas enclosure.
(a) Distortion of structure under its own weight when side panels are removed; the maximum deflection is $130\,\mu$m.
(b) Distortion of structure (with side panels fixed) due to $3\,$mbar overpressure; the maximum deflection is $110\,\mu$m.

pre-installed in a retracted position before the insertion of the beampipe. Access to the fixing bolts for the clamping ring and for both ends of the seal to the VELO is from inside the gas enclosure.

Where gas and light seals are required these are made of Ethylene Propylene Diemo Monomer (EPDM) which has been shown to be compatible with the fluorocarbon gas and is radiation tolerant.

4.2.1 Structural analysis

FEA analysis (Fig. 15) of the rigidity of this structure has demonstrated adequate stability (maximum displacement of $130\,\mu$m) under gravity, when the side panels are removed. With the side panels in place the distortion under gravity is negligible, but the small pressure differential ($\pm 3\,$mbar) results in a maximum displacement of $109\,\mu$m. The stresses in the aluminium structure are negligible.

In the operating configuration the frequency of the first normal mode is around 40-50 Hz. This is close to the frequency of vibrations that might be introduced by nearby pumps, so we will explore the effects of varying the rigidity of the side panels, to change the frequency.

4.3 RICH 1 seal to VELO

The need for a RICH 1 entry window has been eliminated by sealing RICH 1 directly to the VELO outside the acceptance of the detector. The outline requirements for this seal are as follows:

- Light-tight and gas-tight up to $\pm 3\,$mbar gas pressure difference.

- Adjustment tolerance of order $\pm 1\,$mm to accommodate manufacturing tolerances.

Figure 16: RICH 1 seal to VELO.

- Compliance of order ±1 mm to allow thermal, pressure and vibration movements without generating significant forces on RICH 1 or the VELO.

- Entire assembly to be non-magnetic, radiation tolerant, compatible with C_4F_{10}, and should allow RICH 1 and VELO to be electrically isolated.

- Access to both sides of seal to be possible from inside the gas enclosure.

An outline design for this seal is shown in Fig. 16; the drawings in Fig. 31 and Fig. 32 . It comprises a tube, an adjustable collar and a clamp ring, with a compressible EPDM foamed rubber seal providing the necessary compliance. The inner tube is fitted and sealed to the VELO flange. The adjustable collar slides over this and is sealed to it with a sliding O-ring allowing for any set-up error or movement in z. This will also permit small movements in x and y between the VELO and RICH 1 during operation, with a load of 25 kg resulting from 1 mm (the operational stability requirement of the RICH 1 structure is below 0.5 mm) movement of a medium-density foamed seal. The adjustable collar is sealed to RICH 1 with another O-ring and a sliding clamp ring permitting a small x and y misalignment. When fully assembled the loading on both RICH 1 and VELO is nominally zero.

4.4 Exit window and seal to beam pipe

The exit window is a low-mass composite panel made from two 0.5 mm-thick carbon-fibre-reinforced epoxy skins separated by 16 mm thick polymethacrylimide (PMI) foam. Each skin is made from two layers of balanced-weave laminate, with fibres orientated to give 0°/90° in one layer overlapped with ±45° in the other layer. This is in order to generate skins with as close to uniform a stiffness in the plane as possible. The window is to be attached to a flange on the downstream face of the RICH 1 gas enclosure using a clamping arrangement (Fig. 17(b)) that allows for positional adjustment in the x and y directions during assembly. The seal between the window and gas enclosure is made using an EPDM rubber sealing strip. The seal to the beampipe (Fig. 17(a)) uses a compliant annular Kapton film, which has been designed to isolate the window from the beampipe both mechanically and electrically. At the outer edge the Kapton film will be sandwiched between the skins of the window and at the inner edge it will be bonded to a disk on the beampipe using carbon-fibre rings. The assembly drawing for these components
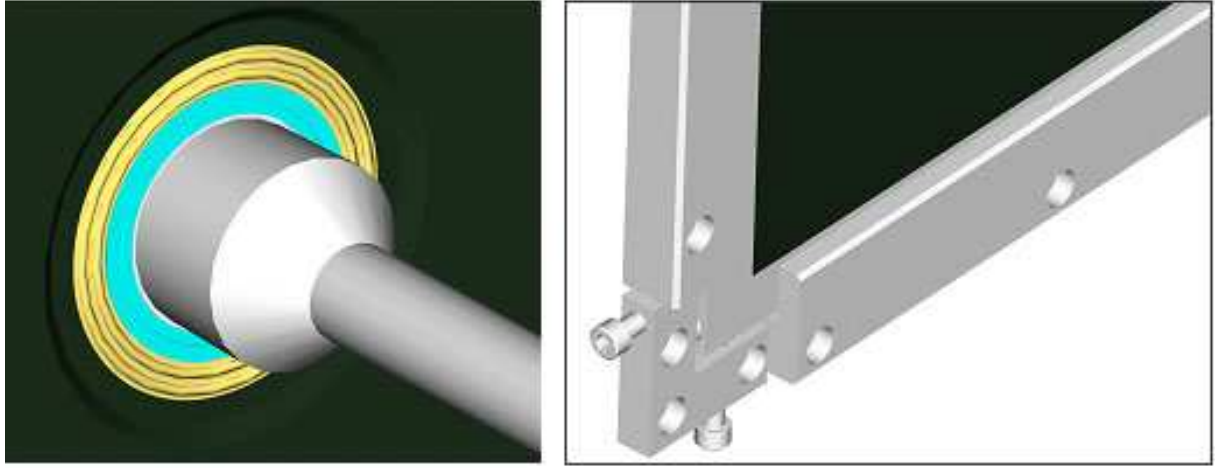
Figure 17: (a) Flexible Kapton seal to the beam pipe, (b) Clamping and adjustment detail.

Table 3: Radiation length of the RICH 1 exit window.

Material	Thickness (mm)	X_0 (mm)	$\%X_0$
CFRP Laminate	1.0	284	0.35
Rohacell 5 IG	16.0	7954	0.20
Epoxy glue	0.4	357	0.11
Total			0.66

is shown in Fig. 33. The methods and procedures were approved at the engineering design review [9] for the LHCb vacuum pipe.

The radiation length of each of the component materials was calculated based on the chemical composition [8]. A breakdown of the calculated radiation length ($\%X_0$) for the RICH 1 exit window is given in Table 3. The figures for the carbon-fibre material are based on the results from a composition analysis of woven pre-cured laminate samples, carried out at RAL. A density of $52\,\mathrm{kg\,m^{-3}}$ was assumed for the PMI foam material, and the epoxy glue figures were based on the RICH 2 epoxy/hardener mix. A one-quarter symmetry model of the RICH 1 exit window was created in ANSYS (Fig. 18) using layered-shell elements. An element formulation specifically designed for modelling sandwich panels was used, which assumes that all of the transverse shear is carried by the core, and that the skins carry none. The material property data used for the carbon-fibre skins was based on the results from a testing programme carried out at RAL. All other properties were taken from manufacturer's data. The window deflection (in z) due to an internal relative gas pressure of $1000\,\mathrm{Pa}$ was calculated. This represents a factor of safety of three on the maximum working overpressure stated for the gas containment. At $300\,\mathrm{Pa}$ overpressure the deflection results in an axial load of $0.4\,\mathrm{kg}$ on the beampipe. A space optimization, shown in Fig. 19, was carried out in order to determine the core thickness associated with the minimum z envelope requirement, which was defined as the thickness of the window plus its deflection in either direction $(t + 2\delta z)$. The optimum core thickness was found to be $16\,\mathrm{mm}$, where the maximum deflection of the window (in z) was $4.3\,\mathrm{mm}$, and factors of safety on stress of 8.8, 18.4, and 15.8 were calculated for the carbon-fibre skins, foam core, and aluminium window frame respectively. Results obtained using this method of analysis compare favourably with test data obtained from a $2\,\mathrm{m}$ x $2\,\mathrm{m}$ prototype panel that was manufactured and tested at RAL.
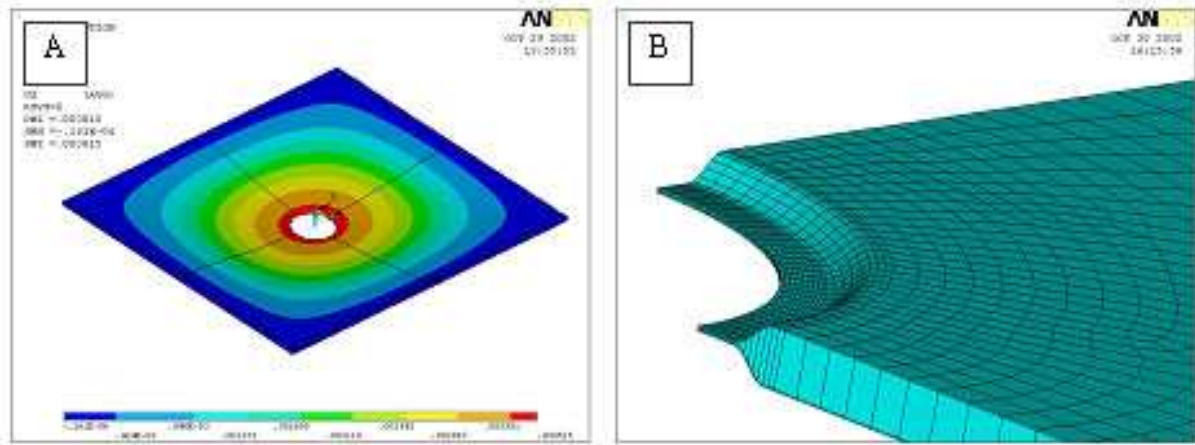
Figure 18: ANSYS model of the RICH 1 exit window.
(a) Contour plot showing deflection of the window (m) due to an internal relative gas pressure of 1000 Pa. The maximum deflection is 4.3 mm.
(b) Detail view of one-quarter symmetry mesh.
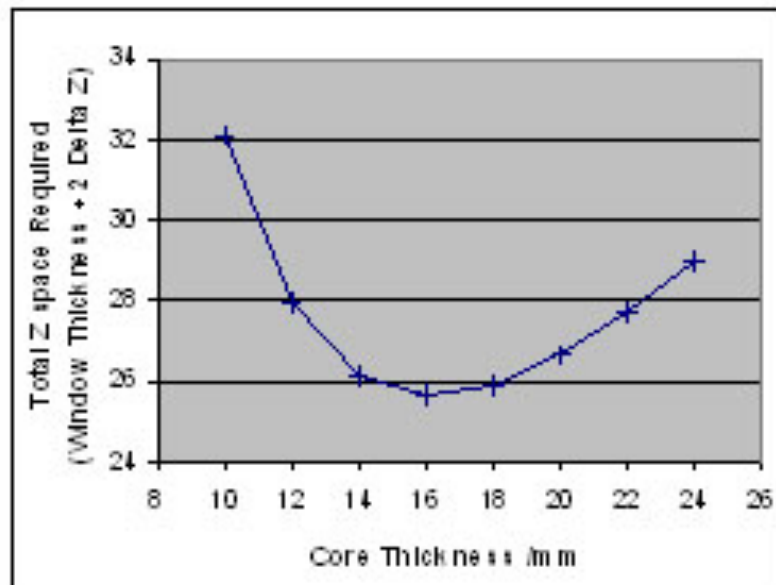
Figure 19: Core thickness optimisation for the RICH1 exit window.

4.5 Quartz windows

The Cherenkov light directed towards the photon detectors must traverse quartz windows approximately 1380 mm×620 mm in area, and 6 mm thick, mounted at the top and bottom of the gas enclosure parallel with the photon detector plane. These form part of the radiator gas containment but offer maximum transparency over the wavelength range of the HPD photocathode sensitivity (200–600 nm). Constraints due to the size of the evaporation plant used to deposit the anti-reflective coating dictate that the windows be constructed from two "panes" of quartz, bonded into a window frame which can be mounted on the gas enclosure with the EPDM seal. The central seam includes a narrow non-magnetic support section, either a T-section integral with the aluminium frame or a separate I-section, which will be of minimal cross section to reduce the shadow on the photon detector plane.

Figure 20: Quartz windows and seal.

A single layer of MgF_2 dielectric anti-reflection coating on a fused silica substrate reduces surface reflectance to under 1.5% per surface over a broad spectral band. A multi-layer coating, optimized for the aerogel Cherenkov light, will be deposited.

A further light and gas-tight seal is provided on the photon detector side of the quartz windows in order to maintain the d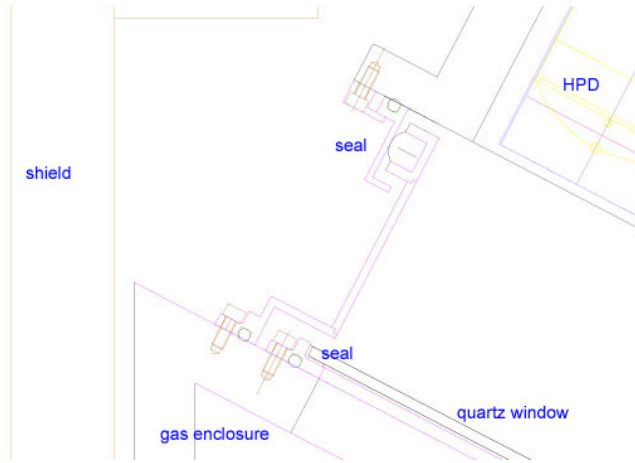ark, nitrogen-filled environment required for the HPDs. This takes the form of a detachable skirt sealed to the HPD assembly, which can be clamped around the window frame. The quartz windows will only be installed along with the other delicate optical components and the apertures will be filled with acrylic or blanking plates during installation and testing. Provision will also be made for the insertion of protective covers when access to the inside of the gas enclosure is required. The quartz windows and seals are shown in Fig.20.

5 Optical elements

5.1 Spherical Mirrors

Cherenkov light is focused onto the photon detector planes using tilted spherical mirrors and a secondary plane of flat mirrors, as shown in Fig.5. The RICH 1 spherical mirrors have a radius of curvature of 2700 mm. The mirror surface is segmented into four rectangular quadrants with a footprint in the $x - y$ projection of the detector system of 795 mm×600 mm. Each quadrant is further segmented and consists of two mirrors. Each of the eight mirrors can be individually adjusted in angle so that the upper and lower segments share a common centre of curvature. The layout of the spherical mirrors is illustrated in Fig. 21. The inner mirrors have a cut-out to accommodate the beampipe. The clearance from the beampipe is yet to be agreed with the beampipe group, but 5 mm is the preferred value. At the time of the LHCb re-optimisation TDR two technologies were under consideration for the spherical mirrors: a carbon-fibre epoxy or glass-coated Beryllium. Due to concerns with regards the long-term stability of the epoxy mirrors in a fluorocarbon environment, the beryllium option has been adopted.

The baseline solution, outlined in the re-optimisation TDR, was to use mirrors composed of a carbon-fibre cyanate-ester-resin material base[3] with an aluminium reflective surface and silicon protective coating. The optical characteristics of a quarter-sized spherical mirror prototype had been examined and found to be within the LHCb figures of merit required for radius of curvature and angular resolution. In addition the reflectivity of a small sample plane mirror

---

[3]Developed and producd by Composite Mirror Applications Inc, Tucson, USA.
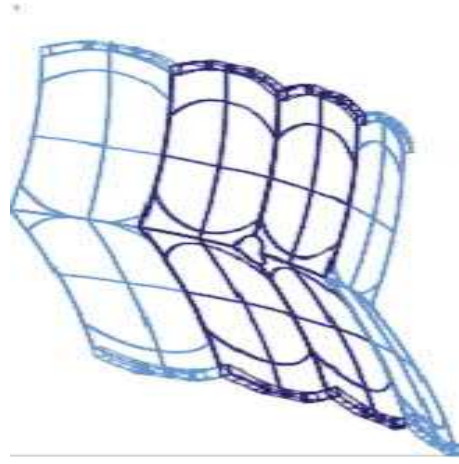
Figure 21: Be Mirror array as viewed from the rear.

had been measured. The reflectivity was found to be approaching the required figure of merit of 90% in the wavelength range of interest ($200 \, \text{nm} < \lambda < 600 \, \text{nm}$) and for the required angles of incidence. With additional tuning of the protective coating material and thickness the figure of merit could be achieved.

An outstanding concern at the time of the re-optimised detector TDR was the suitability of the carbon-fibre composite mirror technology for use in a saturated fluorocarbon environment. The sample plane mirror has subsequently been exposed to a fluorocarbon environment over an eleven-month period. A loss in reflectivity was observed over the period of exposure. This loss has been attributed to carbon fibres from the mirror substrate coming through the aluminium reflective surface; a processes known as print through. This degradation of the mirror is greater than what is acceptable for use in the RICH 1 sub-detector. In addition, the quarter-sized spherical mirror prototype demonstrated a degradation of angular resolution. This degradation occurred with time and in particular with the extra stress placed on the mirror due to the addition of the mirror-to-mirror support mechanical interface cups. The loss of angular resolution exceeded the RICH 1 figure of merit[4] of $D_0 < 2.5 \, \text{mm}$. In contrast, a $6 \, \text{mm}$-thick beryllium prototype mirror, approximately one half the size required for RICH 1, provided a value of $D_0 < 1 \, \text{mm}$ that was stable over time.

5.1.1 Structural analysis

A finite element analysis of a $3 \, \text{mm}$-thick beryllium mirror has been performed [10]. The latest RICH 1 Outer-Mirror design was analysed using ANSYS, paying particular attention to the way in which it will be supported within the detector. Distortions in the spherical mirror surface due to gravity were calculated under a number of support scenarios, using both single pin and two pin mechanisms. In addition, an investigation was made into the stresses and displacements induced in the mirror by preloaded support screws (single point support scheme), thermal expansion (two point support scheme), and misalignment of the mating surfaces at the supports (two point support scheme). The results suggest that compression of the mirror rim due to preloaded support screws is unlikely to cause any significant deformation of the mirror surface. For a double pin support system, careful design would be required to minimise distortions in the mirror due to the misalignment of mating surfaces in the mirror supports, though those caused by a differential thermal expansion between the beryllium mirror and steel

---

[4]D_0 is the diameter of a circular aperture, at the mirror centre of curvature(CoC), in which 95% of light reflected from a point source at the CoC is contained. A D_0 of $2.5 \, \text{mm}$ corresponds to an RMS Cherenkov-angle precision of $0.23 \, \text{mrad}$ for the RICH 1 spherical mirrors.

support structure are tolerable. Given this additional complication a single pin mechanism has been adopted.

Using the surface displacements of the mirror calculated by the FEA, a calculation of the change of the coordinates of the centre of curvature from elemental areas on the mirror surface was calculated by a fitting procedure; this change would be reflected in the final D_0 measurement of the mirror. Results are shown in Fig. 22. A single-pin mount, with a diameter of 10 mm, with zero protrusion beyond the rim of the mirror, gave a maximum deflection on the surface of $174 \, \mu$m; this compares to the best-case scenario, when the full edge of the flange is supported, of $83 \, \mu$m. The mean shift in the x-direction of the centre of curvature was $\sim 20 \, \mu$m with an RMS of $\sim 120 \, \mu$m. The changes in the y-direction were larger with a mean shift of $\sim 700 \, \mu$m with an RMS of $\sim 250 \, \mu$m (corresponding to a D_0 of 2 mm) but still within the tolerances required for RICH 1.

5.1.2 Manufacture

The beryllium-glass mirrors are to be produced by the Russian company Kompozit[5] (the same as has manufactured the LHCb beryllium beampipe). Dish-shaped beryllium blanks, 800 mm diameter and 20 mm thick, are produced by the mining company and sent to Kompozit for machining, grinding and an oxidation process to seal all exposed beryllium surfaces; the glass coating will be performed by the Vavilov State Optical Institute in St Petersburg. A contract has already been placed with Kompozit (June 2004) for the production of a prototype beryllium mirror, which should be delivered by October 2004. This mirror corresponds to the required dimensions of one of the outer RICH 1 mirrors, as shown in Fig. 23(a). The beryllium substrate is 3 mm thick and the glass coating is 0.3 mm. The optical characteristics of this prototype will be tested at CERN, and if the tests are satisfactory it will be used in RICH 1. A contract for the remaining seven beryllium mirrors has been prepared for submission to the ISTC[6]. Production at Kompozit of the seven mirrors will begin as soon as the prototype has been verified. IHEP(Protvino), acts as an intermediary, in accordance with the ISTC rules. The estimated time for production is about 12 months.

5.2 Flat Mirrors

The flat mirrors are of a similar type to those used in the RICH 2 detector. The requirements on the RICH 2 optical designs are more stringent than those of RICH 1 and are therefore compatible.

To cover the flat mirror surface, 16 rectangular mirrors will be used. There will be four panels, one per quadrant, each with four planar mirrors, two mounted above and two below the beampipe. Each quadrant forms a flat mirror. All 16 individual mirrors have the same nominal dimensions of 370 mm (horizontal)×387 mm, and consist of 6 mm-thick Simax glass (borosilicate glass by Sklarny Kavalier). As with the spherical mirrors, there will be a 3 mm clearance between side-to-side mirror segments, resulting in a loss in active reflective surface coverage of about 1.5%.

5.2.1 Manufacture

The Czech company, COMPAS[7], is well qualified to produce the flat mirrors. The same company is producing the mirrors for RICH 2 (60 spherical and 40 flat). Once the RICH 2 mirror

---

[5]Kompozit, Moscow (http://www.korolev.ru/english/e_kompozit.html).
[6]International Science and Technology Centre (http://www.istc.ru).
[7]COMPAS, Research and Development Consortium, Turnov, Czech Republic.
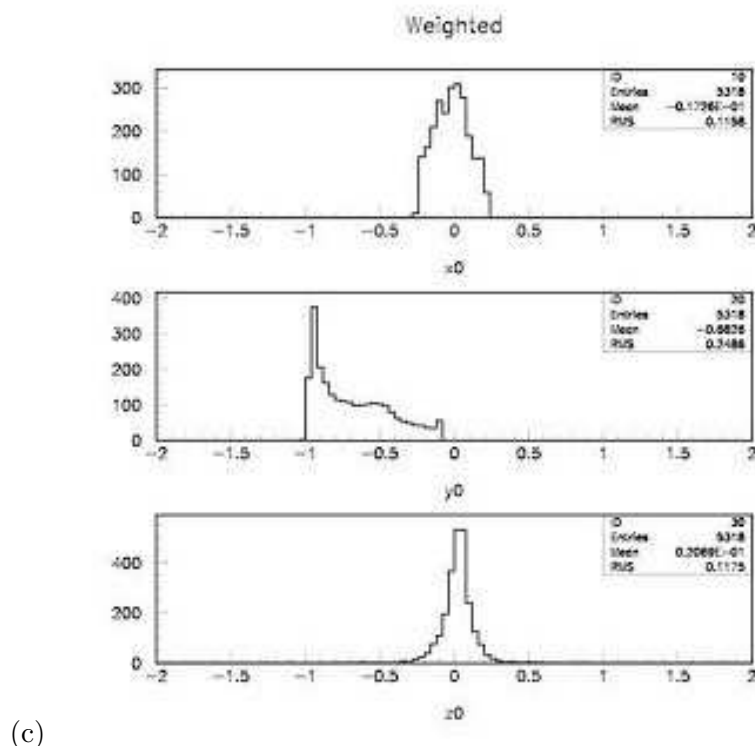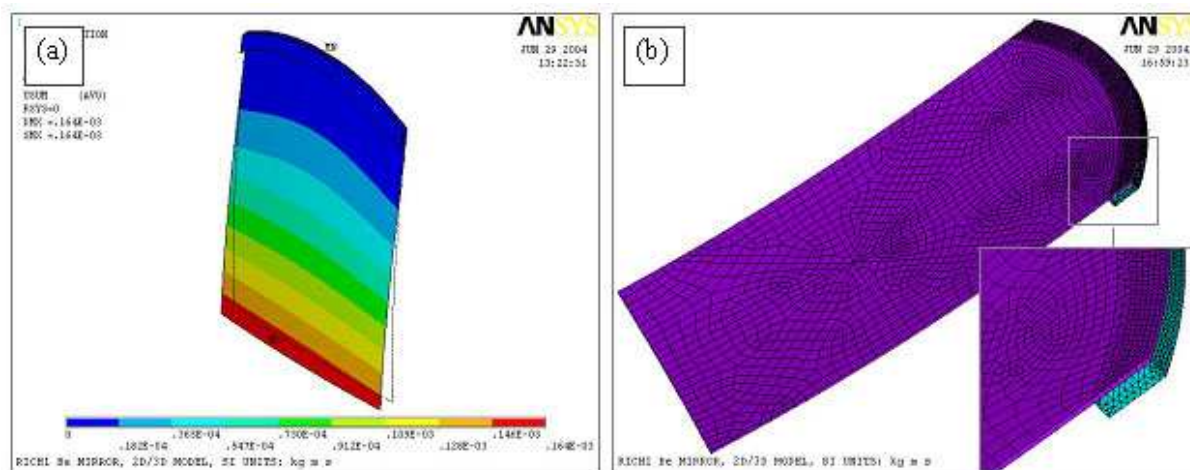
Figure 22: (a) The deflection contour plot from the FEA analysis. The mirror was supported by a single 10 mm pin, (b) The mesh used in the model.
(c) The distribution of the coordinates (in mm) of the centre of curvature of elements of the mirror surface.

production is completed, which is probably by the end of 2004, the RICH 1 16 flat mirror production can begin. Exactly the same production method as for the RICH 2 flat mirrors can be used for the RICH 1 flat mirrors. The timescale for production of the 16 mirrors is about 3 months. The call for tender is foreseen to be sent out in October 2004 and production would begin by February 2005. The 16 flat mirrors would be ready by end of April 2005.

5.3 Spherical Mirror Mounts and Adjustment

The angular resolution of the RICH 1 detector depends on the alignment of its optical components. To ensure that the precision in reconstruction of the Cherenkov angle, about 1.3 mrad in the gas radiator, is not degraded by uncertainties in alignment the aim is to maintain alignment

Figure 23: (a) An outer beryllium mirror, viewed from the rear.
(b) Titanium bushes, inserted into the rim, receive the pins that fix the spherical mirror to its adjustment mechanism. Only the central pin is used to fix the mirror, the outer pins prevent rotation about the central pin.

stability below 0.3mrad. The support design also isolates the mirror from thermal expansion that may otherwise lead to deformation of the mirror profile.

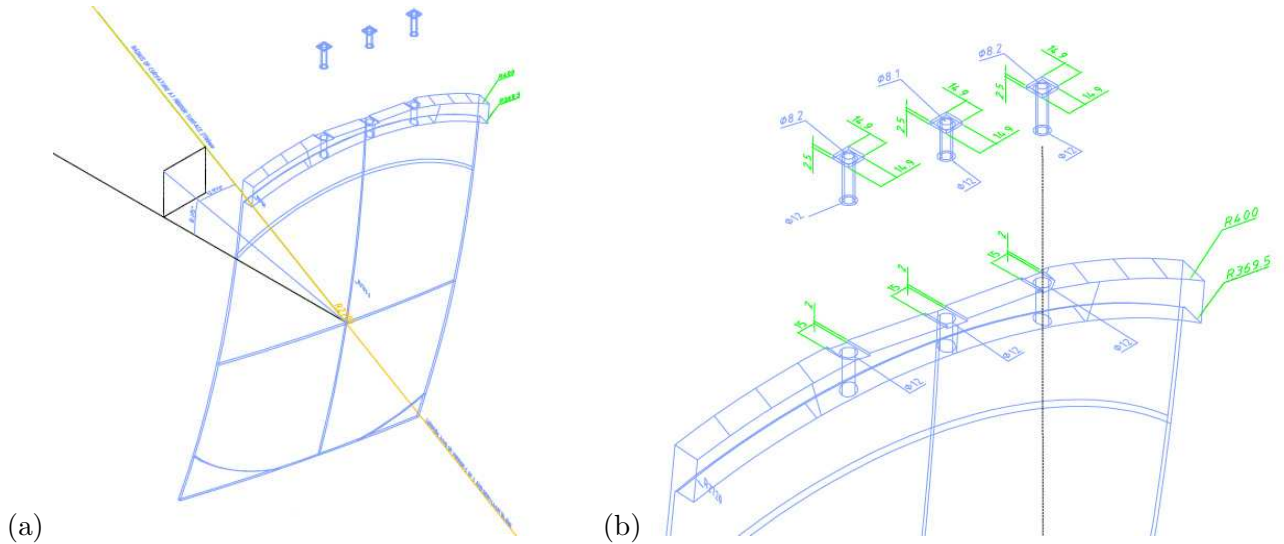There are eight spherical beryllium mirrors arranged in pairs to form four quadrants. Each quadrant forms a spherical mirror surface ($795\,\mathrm{mm}\times600\,\mathrm{mm}$) that can be individually adjusted. The four quadrants are centred on the beampipe. Each mirror is fixed at its $20\,\mathrm{mm}$-thick rim to an L-shaped plate at a central fixed point. Safety requirements preclude any fixing direct to the beryllium so titanium bushes will be inserted in the beryllium, bonded using a radiation-hard glue into holes in the mirror rim, as illustrated in Fig. 23. There is a pin (or pins either end) at the side of the rim as a safety mechanism, to prevent the mirror from rotating about the central fixed-point in case of accidental shocks. The upper mirrors are supported from the top, the lower mirrors have the same but inverted arrangement, therefore are supported from the bottom. The central bushes receive a bolt (or guiding pin) that fixes the mirror to its support frame. A retaining washer in conjunction with the bolt will be used on the inside edge of the rim to ensure the mirror cannot fall or touch the beampipe in the (unlikely) event of poor adherence of the glued bush.

The individual mirror support/adjustment system consists of L-shaped support frames with each quadrant pair of mirrors mounted to a sub frame, which is fixed to the gas enclosure. The L-shaped plates are positioned with the two vertical sides furthest from the beamline, hence outside the detector acceptance. The three adjustable mounts are screwed onto the L-shaped interface plate in the positions shown in Fig. 24. Three threaded spindles are fixed externally at one end by threaded inserts and at the other end terminate at ball joints in the mounts on the L-shaped interface plate. By rotating one or more of the three threaded spindles it is possible to adjust the inclination of the L-shaped interface plates about the horizontal, vertical and one diagonal axis. One of the mounts is fixed in position, while the other two mounts are fitted with sliders. One slider allows motion in the plane of the mirror, the third mount has a degree of freedom in the horizontal axis. The sliders provide the overall mechanism with the ability to isolate the supported mirror from thermal expansion of the gas enclosure.

The long-term stability and adjustment characteristics of the prototype aluminium spherical mirror support have been evaluated. As described in the re-optimisation TDR the relationship
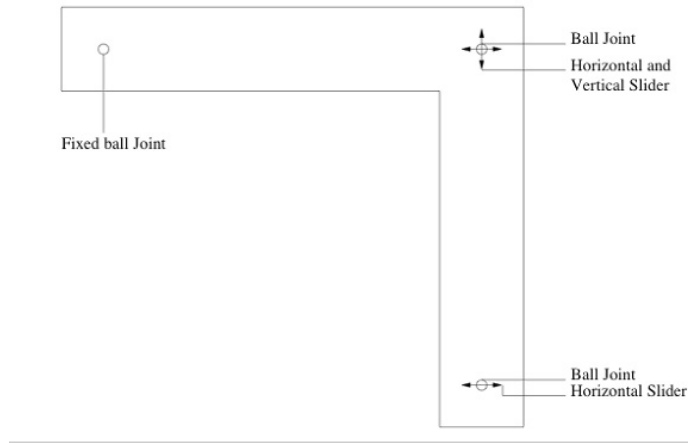
Figure 24: Schematic of the L-shape mirror support frame.
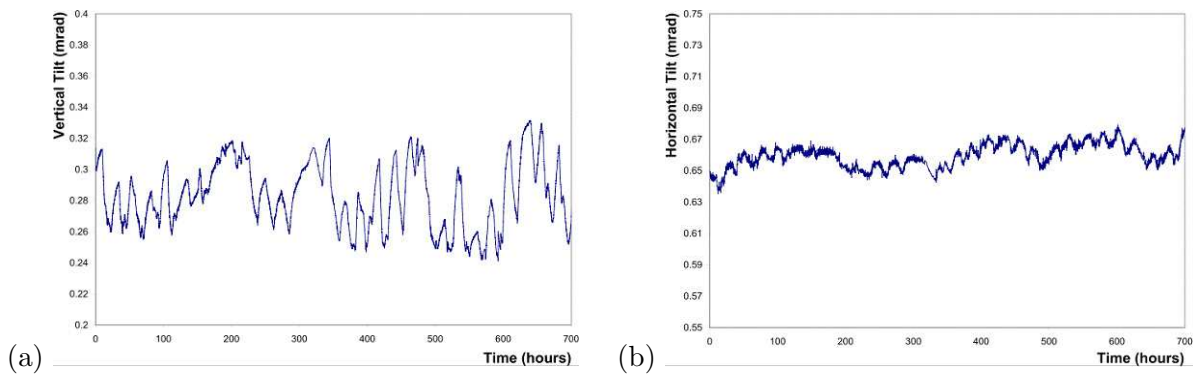
Figure 25: (a) Vertical and (b) horizontal stability measurements of the prototype spherical mirror support over 700 hours.

between mirror tilt and screw-turn is linear. A tilt change of 0.56 mrad corresponds to a screw turn of 36°, which enables a sufficiently precise adjustment. In Fig. 25 the stability of the prototype spherical mirror support over a 700 hour period is shown. In the vertical and the horizontal axes there are fluctuations with a 24 hour period. The range of the vertical tilt is larger than for the horizontal tilt, possibly due to the effects of gravity. The range of the tilt in the horizontal and vertical axes is well below the required 0.3 mrad for RICH 1 requirements. The measurements were taken in a temperature-controlled environment, with a temperature range of 2°C. Further investigations of the support of the mirror support under larger range of temperature fluctuation, 15°C, have been undertaken. The vertical tilt varied over 0.25 mrad whilst the horizontal range was slightly greater than 0.1 mrad. It is expected that this will be reduced with an L-shaped support manufactured from stainless steel, with a lower thermal expansion coefficient. The individual L-shaped mounts for each mirror pair in a particular quadrant are mounted to another intermediate frame (again L-shaped) which is attached to the roof(floor) and sides of the gas enclosure.

5.4 Flat Mirror Mounts and Adjustment

The RICH 1 flat mirrors are outside the LHCb acceptance, so lightweight components are not a requirement. The flat mirrors are of a similar type to those used in the RICH 2 detector and the requirements on the RICH 2 optical designs are more stringent than those of RICH 1. To that end it is proposed to adopt the mirror support of RICH 2. Each mirror segment is fixed on

27

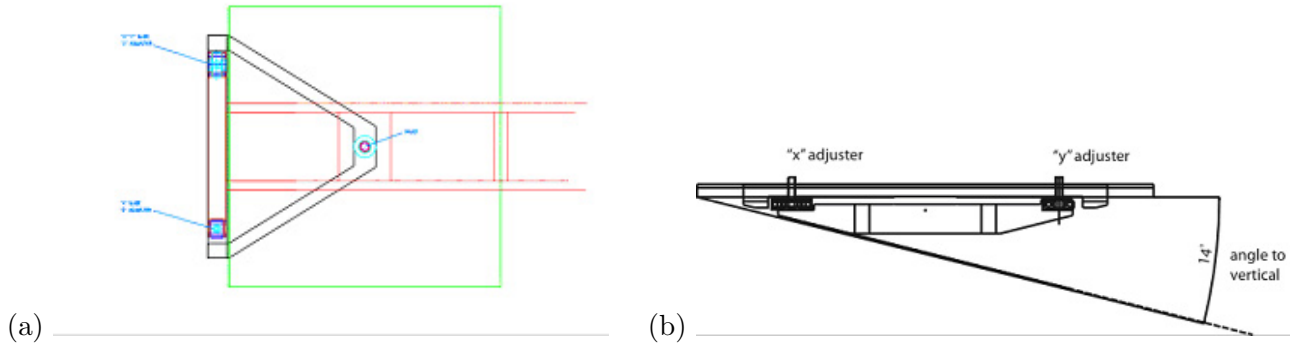Figure 26: (a) Plan view of the mounting mechanism for the flat mirror plane of 4 mirrors. (b) End view of the plane mirror mounting system.

an independent adjustment support that, in turn, is fastened to a panel.

The mirror quadrant panels are 15 mm-thick flat aluminium panels, with a local spotface fine finish at each of the four mirror attachment points and pocketed for each mirror mounting mechanism. The panel is mounted to a triangular support structure positioned behind it (see Fig. 26). There are three support points, a pivot point at the centre of the quadrant and two other points at the quadrant side, allowing for vertical and horizontal tilt adjustment of the quadrant.

Details regarding the flat mirror mountings can be found in the RICH 2 EDR [5]. All flat mirror mounts are identical. Each mount has three attachment points, and each point is adjustable allowing a rotation around the axis defined by the other two attachment points. In this way the four mirrors belonging to the quadrant can be aligned individually to form a single continuous flat mirror surface. The mounts consist of a polycarbonate ring that is glued to the backside of each flat mirror using epoxy. The corresponding polycarbonate tube insert is fixed to the aluminium support panel. Polycarbonate has been chosen because of its compatibility with fluorocarbon gas, low radiation length (though not a requirement for RICH 1), robustness and stability. The ladder element of the plane mirror support, shown in Fig. 26(a), will provide the mounting point to the gas enclosure. The side with the base of the triangular mount slider attachments, is illustrated in Fig. 26(b). The angular sides of the ladder are mounted to a V-shaped frame that is then fixed to the vertical wall of the glass enclosure.

5.5 Alignment

It has been shown that in a misaligned RICH 1 the design angular precision can be recovered using data to align mirrors provided they are physically aligned to about 2 mrad. This corresponds to an accuracy of ~ 0.8 mm in the mirror position.

It is proposed that the mirror alignment will be performed in two stages. Each spherical mirror pair will be aligned to a common centre of curvature outside of the gas enclosure. Similarly each quadrant of the plane mirrors will be adjusted to a common plane. These would then be surveyed for future reference. The mirrors will then be installed in the gas enclosure, outside of the beamline, to align the left and right side spherical mirrors of the upper (and lower) quadrants to a common centre of curvature; similarly the plane mirror quadrants to their respective common planes. This common plane alignment could be achieved by survey with respect to a common mark within the gas enclosure. As the enclosure is not yet installed then the mirror alignment could be verified by illuminating the mirror from a point source close to the z-axis; by covering

28

each half (left/right) it should be possible to align the left and right halves to the same point on the HPD plane. Once the gas enclosure is installed in the beam line the mirrors are re-mounted using the survey marks.

6 Photon Detector assembly

6.1 Overview

The RICH 1 HPD assembly is essentially a copy of the RICH 2 design [5][11]. The mounting of the HPDs and their Mumetal shields, the coupling of the HPDs to the Level-0 readout cards, the circuit boards themselves, their mechanical mounting and their cooling mechanics are identical. The size of the RICH 1 shielding has been chosen to accommodate this design. Differences in the design of the RICH 1 HPD assembly are:

- The number of HPDs is different: 9 columns of 16 HPDs in RICH 2, compared with 7 columns of 14 HPDs in RICH 1.

- The maximum centre-to-centre pitch of the HPDs is 89.5 mm in RICH 2, compared with 91.5 mm in RICH 1. This is to allow the use of 2 mm-thick Mumetal shields if required.

- The routing of the pipes that pass the C_6F_{14} coolant through the cooling plates will be adapted to the RICH 1 HPD nitrogen enclosure.

- The patch panels for cables and services are in the nitrogen enclosure in the RICH 1 design. In RICH 2 they are in the iron magnetic shield.

The above differences are minor details. The main difference is in the rail mounting system and the facilities that are required to remove the HPD assembly from the shield for maintenance.

6.2 Design

The HPD module comprises 7 columns of 14 HPDs, hexagonally close-packed at a pitch of 91.5 mm. Each HPD is fitted with a cylindrical Mumetal shield that protrudes 25 mm beyond the photocathode. The thickness of the Mumetal shield will lie in the range 0.9 mm-2.0 mm, to be decided following magnetic measurements of the shielding. The HPD pins fit into a Zero Insertion Force (ZIF) socket, that is carried by a translator module, a printed circuit board fitted with a flexible kapton foil circuit that plugs onto the Level-0 readout board. The HPD and the ZIF module are shown in Fig 27.

Figure 28 shows the layout of the readout electronics that service the HPDs. This includes the Level-0 boards, the low voltage distribution, then the high voltage distribution for the HPDs. The overall length of the assembly is 610 mm. This assembly is shown (Fig. 29) schematically, within a light-tight nitrogen-filled enclosure, and fitting inside the upper shield box of RICH 1.

6.3 Services

All cables and optical fibres of the readout electronics, including cables from environmental monitoring devices, are connected at a patch panel in the walls of the nitrogen enclosure. They traverse the iron shielding boxes through a 400 mm-wide slot in the side wall (see Fig. 29).
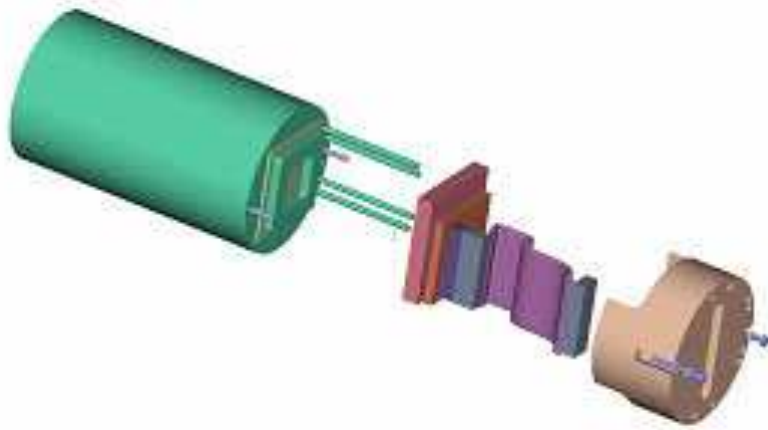
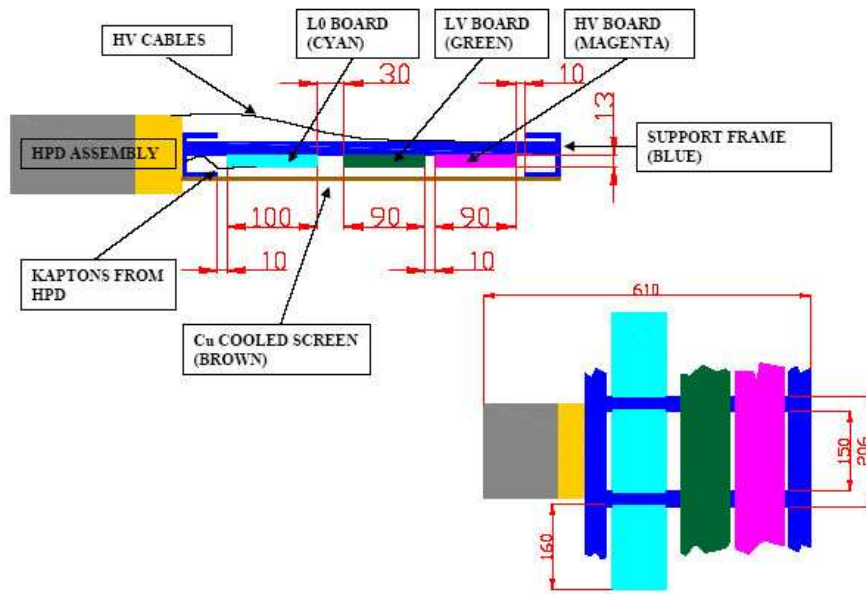Figure 27: Exploded view of HPD and ZIF module.

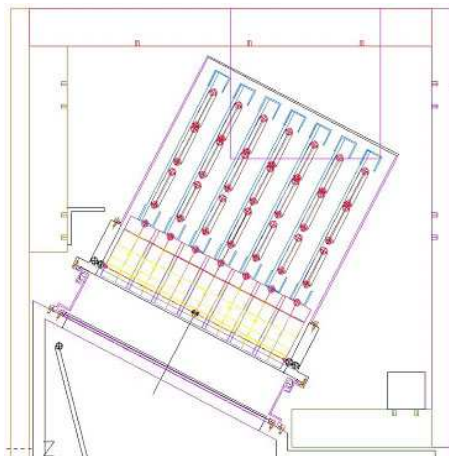Figure 28: Schematic of the HPD and readout assembly.

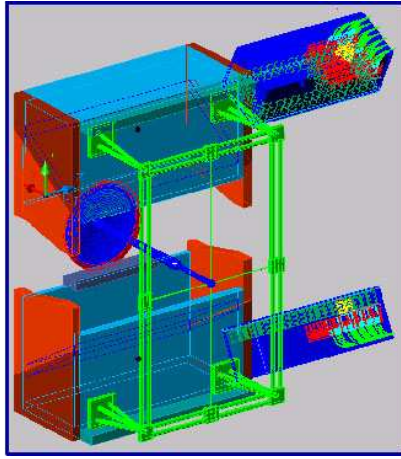Figure 29: Schematic of the HPD assembly inside the upper RICH 1 shield.

Figure 30: Concept of HPD assembly servicing.

Nitrogen is used in the HPD box to avoid high voltage breakdown. A simple system with a single inlet and outlet, flowmeter and pressure probe is used. The flow rate will be about 200 l/hr through the box, maintaining a small overpressure of about 1 mbar.

The power generated inside each HPD module is about 1.5 kW. Active cooling is needed, and C_6F_{14} liquid monophase coolant is used. A single cooling system is provided by the LHC cooling group and is used for RICH 1 and RICH 2. The coolant enters the HPD box at a temperature of $10°$ and pressure of 1.5 bar. The flow rate required is about 3000 l/hr. Inside the HPD module, a manifold distributes the coolant to cooling plates in close proximity to the hot electronic components carried by the Level-0 readout and low voltage distribution boards. The plates are shown in Fig. 28. They are made from a sandwich of aluminium honeycomb with 0.5 mm-thick copper skins, through which two copper pipes carry the coolant. Thermal contact between this plate and the hot components is made using an adhesive thermal pad (Thermagon or similar). The thermal calculations of this design indicate that the HPDs will operate at a temperature close to $15°$. The inlet and outlet coolant pipes will enter and leave the HPD box at the opposite side from the cables. Unlike the cables, the coolant pipes will be disconnected when the HPD assemblies are withdrawn for servicing.

6.4   Access and Maintenance

Within the HPD assembly, servicing and removal of HPDs and other components follows the same procedure as described for RICH 2 in [5]. Accessing the HPD assembly itself, when it is inside the iron shield, is non-trivial and facilities need to be provided. The side panels of the shield (on both sides) need to be removed. This requires lifting gear that can handle up to one tonne. The HPD assembly is mounted on rails and, after disconnecting the coolant and nitrogen pipes, it can be withdrawn along x in the direction of the cables. Extension rails are mounted outside the shield box, lined up with the interior rails. The module can then be withdrawn, with cables attached to its service position. The upper access system will also require a service platform for personnel. The lower assembly will also need to be inverted by rotating it about a horizonatal axis to aid servicing. The concept of the system is shown in Fig 30, though it is preferred to access the upper and lower assemblies from opposite sides of RICH 1.

7 Radiators

7.1 Aerogel

High clarity silica aerogel tiles of dimension $200\,\text{mm} \times 200\,\text{mm} \times 50\,\text{mm}$ and refractive index $n = 1.03$ are currently being produced by the Boreskov Institute of Catalysis in collaboration with the Budker Institute of Nuclear Physics in Novosibirsk. The tiles are mounted in two enclosures and placed around the beampipe at a distance of $50\,\text{mm}$ from the nominal beam line and with the upstream face at $z = 1060\,\text{mm}$. The tiles cover the particle acceptance area of $600\,\text{mm} \times 500\,\text{mm}$. The downstream face of the enclosure is made from a $100\,\mu\text{m}$-thick glass (Schott D263 T) filter that absorbs UV photons above about $4\,\text{eV}$, which are most affected by Rayleigh scattering. The upstream face is a thin black kapton sheet to absorb Cherenkov light from the gas upstream of the aerogel.

The aerogel is hygroscopic and needs to be stored in a dry nitrogen atmosphere. Within the RICH 1 gas volume the aerogel enclosure will be a nitrogen atmosphere, kept at the same pressure as the C_4F_{10} gas. The experience of the HERMES experiment, that has run with aerogel enclosed in nitrogen, inside a C_4F_{10} gas volume during several years, indicates that there are no strict requirements on the gas tightness of the aerogel enclosure.

The Milano team has conducted a long and intensive R&D programme with this aerogel, involving radiation hardness tests, optical characterization in the laboratory and with charged particle beams. The results are reported in Chapter 4.3 of [1] and references therein.

7.2 C_4F_{10} gas

The RICH 1 gas radiator, C_4F_{10} has a refractive index at cavern temperature and pressure that is well described by a Sellmeir formula

$$(n-1) \times 10^6 = \frac{0.2375}{73.63^{-2} - \lambda^{-2}} \ ,$$

with λ the wavelength in nm.

The gas volume is about $5\,\text{m}^3$. More than $2\,\text{tonnes}$ of C_4F_{10} has been purchased owing to the closing down of the production line by the 3M company. This stock correponds to about $200\,\text{m}^3$ or 40 fillings of RICH 1. Taking account of the DELPHI and COMPASS experience that a loss of about 1-2 kg per day can be expected due to leaks, our supply should last several years of normal LHCb operation.

The LHC gas systems are considered as a service to the experiments. As such the C_4F_{10} gas system for RICH 1 is not a RICH group deliverable. The gas group is responsible for its operation, control and safety, and for ensuring the required level of impurities (nitrogen$\sim$1%, water vapour and oxygen$<$100 ppm). The system design has not changed significantly from that presented [12] at the time of the RICH TDR.

8 Alignment, Monitoring and Control

While it has been demonstrated through simulation that optical alignment parameters and refractive index of the radiator gas can be monitored and corrected using data, it is desirable to provide hardware features as well. These devices contribute to the RICH Detector Control System (DCS), itself part of the LHCb ECS (Experimental Control System). The RICH DCS

is described in detail elsewhere [13][14]. The items relevant to the RICH 1 engineering design are summarized here.

The parameters that need to be monitored can be grouped as follows:

- *Environmental monitoring:* Temperature, humidity, pressure, mechanical vibration and magnetic field, are measured in the gas enclosure and HPD assemblies. The various sensors are routed to Embedded Local Monitorong control Boards (ELMB). The ELMBs have 64 ADC channels and are tolerant to radiation and magnetic fields. RICH 1 requires a total of 330 temperature sensors, 8 humidity sensors, 4 pressure sensors, 4 magnetic probes and 2 accelerometers. These can be serviced using 7 ELMBs.

- *Safety interlocks:* These are based on Programmable Logic Controllers (PLC) in a closed loop, that switch off power in the event of overheating. Two Pt100s in each HPD box are hardwired to the PLC in the control room. A temperature reading above threshold will automatically switch off power to the HPD assemblies.

- *Quality monitoring:* This includes monitoring of the C_4F_{10} gas refractive index and transparency and mirror alignment.

  Gas Quality:
  Impurities in the C_4F_{10} gas should be below 100ppm for oxygen and water, while nitrogen should be constant and below 1%. An ultrasound velocity measurement device has demonstrated that it can measure the nitrogen concentration in C_4F_{10} with a precision better than 1%. A spectrophotometer can measure the concentration of absorbing impurities in the gas. In the wavelength range 160-180 nm, oxygen and water vapour show strong absorption.

  Mirror alignment:
  A laser and CCD system will be placed in the RICH vessel to monitor movement of the mirror segments. A beam is split, one half reflected from the mirror segment to the CCD, while the other travels direct to the CCD. A measurement of the distance between the two images separates out a true mirror displacement from movement of the monitoring system. The system is described in reference [13].

- *Calibration:* An important calibration task is the measurement of the magnetic field induced distortions of the HPD electron optics. The image of a pin-hole grid mask is projected onto the HPD plane with the LHCb dipole magnet off. The image displacements measured when the magnet is on are used to calculate the HPD distortion corrections.

9 Assembly and Installation procedures

The installation and assembly of the components of RICH 1 is subject to many constraints, both temporal and spatial. A sequence of procedures needs to be followed that involve not only the components of RICH 1, but also its neighbouring sub-detectors, the VELO, the beampipe and the TT station. Furthermore, space is very limited at the location of RICH 1, the cavern crane is not accessible and lifting height above RICH severely restricted. After installation, access must be provided to the HPD assembly and the optical components and to the beampipe for bake-out, so appropriate procedures and tooling are required.

9.1 Installation sequence and schedule

1. Magnetic shields   April 2005

- The upper and lower magnetic shields are mechanically linked with vertical beams and moved from the cavern into the tunnel area using skates (caterpillers).

- Lower shield is fixed to the floor, upper shield to the cavern wall.

- Support beams are removed and shields aligned to nominal beam line ($\sim 1\,\mathrm{mm}$ precision).

2. Gas enclosure   December 2005

- A temporary rail is installed on upper shield.

- All detachable panels and windows are removed.

- Enclosure is inserted and fixed to lower shield

- Enclosure is tilted and aligned to nominal beamline ($\sim 1\,\mathrm{mm}$ precision).

3. The beampipe   January-July 2006

- VELO tank must be in place.

- Support for downstream end of beampipe is provided.

- Support table inside gas enclosure is provided.

- Beampipe is inserted through gas enclosure, aligned to nominal beamline and clamped to VELO tank.

- Seal to VELO tank is made. Access to both sides of seal is from inside gas vessel.

- Exit window is threaded over beampipe and aligned.

- Kapton seal is glued to beampipe

- Exit window is sealed to gas enclosure.

- Vacuum pipe is baked out.

4. Optical components   July 2006

- Shield side panels and gas enclosure side panels are removed.

- Spherical mirrors are installed in sub-assemblies of two (one quadrant).

- Plane mirrors are installed in sub-assemblies of four (one quadrant).

- Aerogel radiator is mounted in two parts around beampipe.

- Final mirror alignment using survey targets ($0.5\,\mathrm{mm}$ precision).

5. Photon detectors   July-October 2006

- Temporary rails are fixed to upper and lower shields.

- Shield side panels are removed.

- Upper and lower HPD assemblies are mounted on temporary rails.

- Cables and services (nitrogen and flourocarbon cooling) are attached.

- HPD assemblies are inserted by transfer from temporary rails to fixed rails in shielding, then locked into position ($0.5\,\mathrm{mm}$ precision).

- Photon funnel is sealed to quartz window.

- Shield side panels are replaced

- Temporary rails are removed (only if necessary).

9.2 Installation tooling required

- Installation support beams to mount upper shield from lower.

- Skates to move shield from cavern to final location.

- Lifting device for shield side panels (approx 1 tonne).

- Gas enclosure installation rail.

- Beampipe installation working table.

- Supports for "threaded" components, viz: beampipe clamping ring, VELO seal and exit windows.

- Flat and spherical mirror handling tools.

- Aerogel mounting tools.

- HPD module installation/access rails.

- Upper HPD access platform.

- Protection plates for quartz windows.

- HPD cable-harness transport.

While working solutions exist for all the major challenges the detailed design work for many of these items has yet to be done.

10 Project planning

The following lists indicate the institutes responsible for delivery of the various work packages and their schedules.

1. Shielding:

Critical date: Installed in time for Magnet measurements with shields in 2005

1.1	Main dimensions defined	Imperial	April 2004
1.2	Magnetic performance	Imperial	May 2004
1.3	Envelope	Imperial	April 2004
1.4	Mechanical design	Imperial	May 2004
1.5	Details:		May 2004
	a) cable window	Imperial	
	b) cooling-pipe window	Imperial	
	c) mounting points for HPD support	Imperial	
	d) mounting points for gas vessel support	Imperial	
	e) front teeth	Imperial	
	f) shelf	Imperial	
	g) mounting from cavern wall	CERN	
	h) mounting from floor	CERN	
	i) craning points	CERN	
1.6	FEA	CERN	May-July 2004
1.7	Production Drawings	CERN	May-July 2004
1.8	PRR		Aug 2004

1.9	Tender/order	CERN	Aug/Sept 2004
1.10	Manufacture		Oct-March 2005
1.11	Installation	CERN	April 2005
1.12	Magnetic tests	CERN/Imperial	??? 2005

2. Gas Enclosure:

Critical dates:
> begin assembly July 2005
> ready for installation Nov 2005

2.1	Design		May-Sept 2004
	a) interface with shielding	Imperial	
	b) installation procedure	Imperial	
	c) finalize optical parameters	Imperial	July 2004
	d) interface with flat-mirror support	Imperial/Bristol	
	e) interface with spherical-mirror support	Imperial/Bristol	
	f) interface with aerogel support	Imperial/Milano	
	g) flange to quartz window	Imperial/Oxford/RAL	
	h) flange to side panels	Imperial/Oxford	
	i) flange to exit window	Imperial/Oxford/RAL	
	j) flange to VELO seal	Imperial/Oxford/RAL	
	k) interface to gas system	Imperial/CERN	
2.2	FEA	Oxford/RAL	Sept 2004
2.3	Production drawings	Oxford/RAL	Aug-Oct 2004
2.4	PRR		Nov 2004
2.5	Tender/order	Imp/Oxford/RAL	Dec 2004
2.6	Manufacture		Jan-June 2005
2.7	Assembly tooling	Imperial	
2.8	Assemble in B156	Imp/Oxford/RAL	July-Oct 2005
2.9	Install in IP8	Imperial/CERN	Nov 2005

3. Spherical Mirrors:

Critical dates:
> order production mirrors December 2004
> assembly tests September 2005
> Installation July 2006

Beryllium mirrors will be manufactured through IHEP/Kompozit

3.1 Be mirrors (8 required)		
a) prototype mirror order	CERN	May 2004
b) define final parameters	Bristol/CERN	July 2004
c) prototype delivered		Oct 2004
d) prototype testing	Bristol/CERN	Oct-Dec 2004
e) PRR		Dec 2004
f) order production mirrors	CERN	Dec 2004
e) test production mirrors	Bristol/CERN	Jun-Aug 2005
f) assembly tooling	Bristol/Imperial	
g) assembly in B156	Bristol	Sept-Oct 2005
h) installation at IP8	Bristol/Imperial	July 2006
3.2 Be mirror supports		
a) Design/prototyping	Bristol/Imperial	May-Oct 2004
b) production drawings	Bristol	Nov-Dec 2004
c) PRR		Dec 2004

| | d) manufacture | Bristol | Jan-June 2005 |
| | e) assembly in B156 | Bristol | Sept-Oct 2005 |

4. Flat Mirrors:

Critical dates:

       Assembly tests september 2005

       Installation July 2006

The 16 plane glass mirrors will be the same technology as RICH 2 plane mirrors and their supports could be made using same technology.

4.1	Order plane mirrors	Bristol/CERN	Oct 2004
4.2	Test mirrors	Bristol/CERN	May-June 2005
4.3	Assembly in B156	Bristol	Sept-Oct 2005
4.4	Installation at IP8	Bristol/Imperial	July 2006

5. Aerogel

Parameters (dimensions and refractive index) defined

Manufacture at Novosibirst inst of catalysis

Critical dates:

       Support ready for assembly September 2005

       Ready for installation in Sept 2006

5.1	Manufacture of tiles	Milano/Novosibirsk	July 2004-July 2005
5.2	Testing of tiles	Milano	Jan - Dec 2005
5.3	Manufacture of support	Milano/Imperial	Mar-May 2005
5.4	Assembly of support	Milano/Imperial	Aug 2005
5.5	Installation in RICH1	Milano/Imperial	Sept 2006

6. Quartz Windows

Will use identical technology to RICH 2 (joint order considered)

Critical date: Installation July 2006

6.1	Design	Imperial	Oct - Dec 2004
6.2	Production drawings	Imperial	Jan - Feb 2005
6.3	PRR		Feb 2005
6.4	Manufacture		Mar-Sept 2005
6.4	Antireflective coating	CERN	Dec 2005
6.5	Assemble	Imperial	Jan-Feb 2006
6.6	Install at IP8	Imperial	Not before July 2006

7. VELO seal

Critical dates:

       Assembly tests August 2005

       Installation Jan 2006

7.1	Design and prototyping	RAL/Imperial	May - Jan 2005
7.2	PRR		Feb 2005
7.3	Manufacture	RAL	Feb - June 2006
7.4	Assemble in B156	RAL/Imperial	Aug 2005
7.6	Install at IP8	RAL/Imperial	Jan 2006

8. Exit window

Critical dates:

	Assembly tests September 2005		
	Installation Feb 2006		
8.1	Design and prototyping	RAL/Imperial	May - Jan 2005
8.2	PRR		Feb 2005
8.3	Manufacture	RAL	Mar - Aug 2005
8.4	Assemble in B156	RAL/Imperial	Sept 2005
8.5	Installation in IP8	RAL/Imperial/CERN	Feb 2006

9. HPD Assemblies: including cooling and maintenance assemblies

Aim to use as much as possible of the RICH2 HPD assembly design
The cooling system is shared with RICH2
Critical dates:

      HPD support ready to receive modules January 2006   Installation Aug 2006

Depending on HPD delivery it may be necessary to install up to 50% of HPDs
during the commissioning phase (post September 2006)

9.1	Cooling system design	CERN	Jan - June 2004
9.2	Tender / order cooling system	CERN	June - Dec 2004
9.3	Mechanics design	Imperial	Oct - Feb 2005
9.4	Production drawings	Imperial	Jan - Mar 2005
9.4	Mechanics PRR	Apr 2005	
9.5	Install cooling system	CERN	June - Oct 2005
9.6	Manufacture mechanics	Imperial	May - Nov 2005
9.7	Assemble HPD modules	Imperial	Jan - July 2006
9.8	Installation of HPD modules	Imperial/CERN	Aug 2006

10. Monitoring and Alignment Facilities

Institute responsibilities in this area are still under discussion, with interest
expressed as indicated:

10.1	Mirror alignment hardware and software	Bristol/Glasgow/Imperial/RAL
10.2	Environmental monitoring	RAL
10.3	Gas quality monitoring	RAL
10.4	HPD B-field calibration	CERN
10.5	Detector safety interlocks	???
10.6	High and low voltage supply monitors	CERN/Genova/Milano
10.7	readout electronics monitoring	Cambridge/Oxford
10.8	DCS and PVSS architecture	RAL

11. Handling tools, maintenance and access facilities

Critical dates:

      As required for installation of shields at IP8: Jan-Feb 2005
      As required to execute assembly tests in B156: July-Nov 2005
      As required to facilitate installation at IP8: Dec 2005-July 2006

11.1	Transport of shields to IP8 - 16 tonnes	CERN
11.2	Tools for insertion /removal of spherical mirrors - 20 kg	Imperial/Bristol
11.3	Tools for insertion/removal of plane mirrors - 25 kg	Imperial/Bristol
11.4	Tools for insertion/removal of Aerogel - 2 kg	Imperial/Milano
11.5	Tools for installation and support of beam-pipe - 20 kg	CERN/Imperial
11.6	Tools for insertion and sealing exit window - 50 kg	RAL/Imperial
11.7	Rail structure to access and maintain HPDs - 500 kg	Imperial/CERN
11.8	Installation procedures for above	

References

[1] LHCb Collaboration, R. Antunes Nobrega *et al.*, LHCb Reoptimized Detector, Technical Design Report, CERN–LHCC/2003–30.

[2] LHCb Collaboration, S. Amato *et al.*, RICH Technical Design Report, CERN–LHCC/2000–37.

[3] LHCb: Addendum to the RICH TDR, CERN–LHCC/2003–59

[4] RICH photon detector readout electronics Review Report, EDMS: 460946.

[5] M. Adinolfi *et al.* LHCb RICH 2 Engineering Design Review Report, LHCb–EDR/2002–9.

[6] LHCb Detector Geometry database, EDMS: 330689 (ver 4.0).

[7] LHCb Collaboration, R. Antunes Nobrega *et al.*, LHCb Trigger, Technical Design Report, CERN–LHCC/2003–31.

[8] P. Loveridge, A. Papanestis, Radiation Length Calculations for the RICH 2 Composite Radiation Windows, EDMS 495184, April 2003.

[9] Engineering Design Review for the LHCb beampipe, EDMS 398556, September 2003.

[10] P. Loveridge, RICH 1 Beryllium Mirrors: A Finite Element Study, EDMS 485429, July 2004.

[11] J.Bibby *et al*, The Readout Electronics of the LHCb RICH Detector, Electronics System Review, EDMS 492255.

[12] M.Bosteels *et al*, LHCb RICH gas systems, LHCb 2000-079.

[13] C.D'Ambrosio *et al*, Monitoring, Alignment and Control of the RICH detectors, LHCb 2000-080.

[14] F.Metlica *et al*, The LHCb RICH Detector Control System: draft note: http://fmetlica.home.cern.ch/fmetlica/Talks/DCSnoteproposal.doc

11 Detailed drawings

1. RICH 1 seal to VELO.

2. RICH 1 seal to VELO assembly.

3. RICH 1 exit window assembly.

Figure 31: RICH 1 seal to VELO.
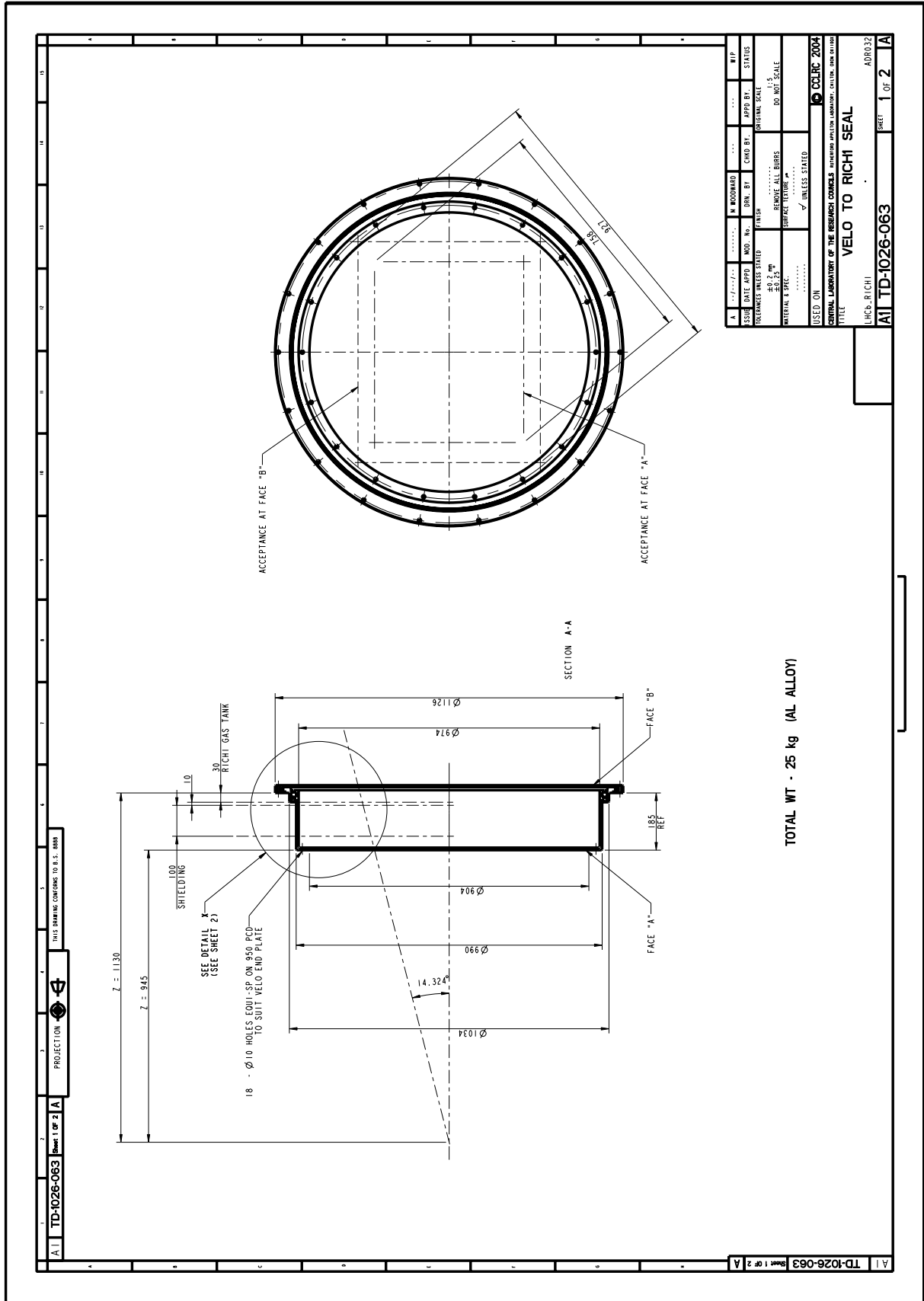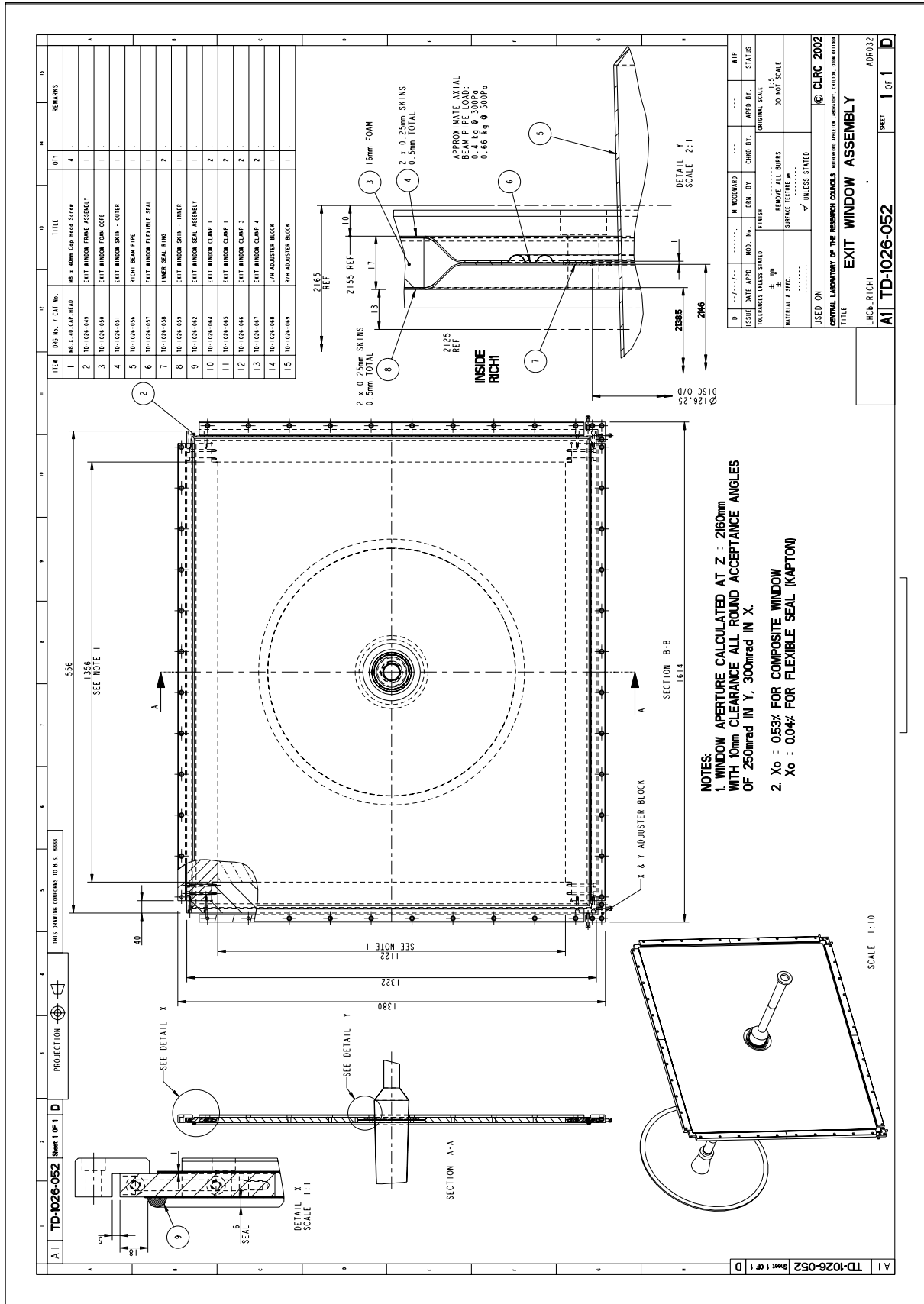
Figure 32: RICH 1 seal to VELO - assembly drawing.

Figure 33: assembly drawing for exit window.